Thomas Drescher

Zero Modes in Compact Lattice QED

Diplomarbeit
zur Erlangung des Magistergrades der Naturwissenschaften
verfaßt am Institut für Theoretische Physik
an der Karl-Franzens-Universität Graz
Betreuer: Univ.-Prof. Dr. C. B. Lang
Graz, 2003

Meinen Eltern gewidmet

Contents

Chapter 1

Introduction

In the 1940's quantum electrodynamics (QED), the quantum field theory of electromagnetism, became fully developed by Freeman J. Dyson, Richard P. Feynman and Julian S. Schwinger in the United States and Shinichiro Tomonaga in Japan. QED deals with processes involving the creation of elementary particles from electromagnetic energy, and with the reverse processes in which a particle and its antiparticle annihilate each other and produce energy. The fundamental equations of QED apply to the emission and absorption of photons by atoms and the basic interactions of photons with electrons and other elementary particles. These photons are virtual; that is, they cannot be seen or detected in any way because their existence violates the conservation of energy and momentum. The particle exchange is merely the force of the interaction. Nowadays QED is part of the standard electroweak model [1–3], which describes all phenomena of both the electromagnetic and weak interactions in the presently known energy range.

An important feature of QED (as well as of QCD) is the invariance under local symmetry transformations. The local symmetry group is a continuous one; it is the well known Abelian group $U(1)$.

In principle, QED is able to describe the electromagnetic interactions of charged particles with high accuracy within the framework of renormalizable continuum perturbation theory. This is a result of the marginal strength of the coupling constant. Thus, the study of lattice QED can neither be motivated by as yet unexplained phenomena nor by a lack of computational methods. But still there are several reasons why people study lattice QED:

- Compact lattice QED is the simplest (Abelian) gauge theory and may serve as the prototype for all compact gauge theories on the lattice in 4 dimensions. It exhibits a twofold phase structure, separated by a mass gap: one phase with a massless particle, the photon, called

the Coulomb phase and one phase which shows confining. Though the QED confining phase is unphysical and is not realized in nature we can probably learn something which will be useful in other theories showing confinement (like QCD).

- Studying the phase transition behavior of QED will give useful information for other theories exhibiting phase transitions as well. To understand the behavior and occurrence of phase transitions is also an important subarea of statistical mechanics.

- In the confining region, where the coupling becomes strong, various topological objects can be observed, like monopoles, Dirac sheets, Dirac plaquettes, toron charges etc. Their possible connection to the appearance of zero modes of the Dirac operator is of special interest.

- An apparent mathematical inconsistency in QED is the occurrence of so called Landau poles in the perturbation regime of the renormalized coupling constant. This pole would be absent if QED would have an ultraviolet stable fixed point for the running coupling outside the perturbation region. The lattice provides a non-perturbative formulation and seems thus to be a proper way to study the Landau pole problem.

Another not less important aspect is the numerical effort in computer simulations. Since numerical investigations of Abelian models are much easier and faster than for other more complicated gauge groups, studying the U(1) model may provide useful results applicable to more general theories.

1.1 Overview

The thesis is organized as follows. The next chapter is supposed to be a short recapitulation of the QED basics in the continuum, including the introduction of Euclidean space-time and an explanation of the Landau pole problem.

In the third chapter the lattice is introduced as a regularization scheme and some lattice operations are defined. Being familiar with the lattice basics we can discretize the gauge field part and the fermion part of the QED action. When discretizing the fermion part a problem, called the fermion doubling problem, occurs. Light is shed on this unwanted phenomenon before several ways leading more or less out of this dilemma are discussed. Thereafter attention is given to renormalization on the lattice and the phase structure of compact lattice QED. The Metropolis method for updating the gauge fields is discussed.

In chapter 4 Dirac operators which overcome the fermion doubling problem while still perpetuating chiral symmetry are covered. One of these solutions is called the chirally improved Dirac operator. As I have done some calculations on it this operator will be discussed in more detail.

Chapter 5 deals with the ideas and methods one can use in order to extract physical relevant results. The importance of studying the gauge fields as well as the zero momentum modes is shown and possibilities to bring the results in relation are discussed.

The sixth chapter is devoted to the presentation and discussion of the obtained results.

In the last chapter the obtained results are summarized and suggestions for further studies are given.

Chapter 2

Continuum formulation

This chapter ought to be a summary of quantum electrodynamics in the continuum. The intention is after the discretization of space-time, maintaining as many continuum symmetries as possible and taking the limit of infinitesimal small lattice spacing to finally again attain at the results presented here.

2.1 QED in the continuum

The QED action in the continuum [4]

$$S_{\mathrm{QED}} = -S_{\mathrm{G}} + S_{\mathrm{F}} \tag{2.1}$$

consists of the pure gauge field part S_{G}

$$S_{\mathrm{G}} = \frac{1}{4e^2} \int d^4x \; F_{\mu\nu} F^{\mu\nu} \tag{2.2}$$

and the fermion part S_{F}

$$S_{\mathrm{F}} = \int d^4x \; \bar{\psi}(x)(i\,\gamma^\mu\,\mathcal{D}_\mu - M)\psi(x), \tag{2.3}$$

where $F_{\mu\nu} = \partial_\mu A_\nu - \partial_\nu A_\mu$ is the Abelian gauge field strength tensor, $\mathcal{D}_\mu = \partial_\mu + i\,e\,A_\mu$ denotes the covariant derivative and A_μ is the vector potential. M and e denote the bare fermion mass and bare electric charge (or the coupling constant), respectively. Here, $\bar{\psi}(x)$ and $\psi(x)$ represent the fermion fields and obey the rules of Grassmann algebras (see the Appendix). The γ_μ are the 4×4 Dirac matrices satisfying the algebra

$$\{\gamma_\mu, \gamma_\nu\} = 2g^{\mu\nu}, \quad \mu = 0, \ldots, 3.$$

There are two types of Abelian gauge transformations

$$\psi'(x) = e^{-i\,q\,\theta}\psi(x), \qquad \theta \in U(1), \tag{2.4}$$

which can be applied to the fields in (2.1) depending on whether or not θ is a function of x:

$$\begin{array}{rl} \theta = \text{constant} & \text{global gauge transformation} \\ \theta = \theta(x) & \text{local gauge transformation.} \end{array}$$

A global Abelian gauge transformation is defined by

$$\left.\begin{array}{l} \psi(x) \to e^{-i\,q\,\theta}\psi(x) \\ \bar{\psi}(x) \to e^{i\,q\,\theta}\bar{\psi}(x) \end{array}\right\} \text{ complex fields} \qquad A_\mu(x) \to A_\mu(x) \quad \text{real fields,} \tag{2.5}$$

and q can be a different number for each complex field. Later, q will be associated with the electric charge.

If the Lagrangian is invariant under the transformations (2.5), Noether's theorem predicts the conserved quantity

$$J^\mu = q\,\bar{\psi}\,\gamma^\mu\,\psi. \tag{2.6}$$

By identifying $q = e$, this is the electromagnetic current and we may charge conservation interpret as a consequence of a global gauge symmetry of the theory.

Let us now generalize the gauge transformation by requiring θ to depend on the local space-time point, i.e. $\theta = \theta(x)$. The QED-Lagrangian is invariant under the following local Abelian gauge transformations:

$$\begin{array}{c} \psi(x) \to G(x)\psi(x) \\ \bar{\psi}(x) \to \bar{\psi}(x)G^{-1}(x) \\ A_\mu(x) \to A_\mu + \frac{i}{e}\,G(x)\partial_\mu G^{-1}(x). \end{array} \tag{2.7}$$

where

$$G(x) = e^{-i\,e\,\theta(x)}. \tag{2.8}$$

The requirement of local gauge invariance does neither allow for a possible mass term for the vector field nor a possible symmetric field combination to appear in the Lagrangian. Thus, we can infer that *the requirement of local gauge invariance dictates the form of QED.*

2.1.1 Chiral symmetry

The effect of breaking chiral symmetry is a key feature of the theory of strong interactions, QCD. This theory is in the confining phase for all values of the coupling constant. We shall see a bit later that QED also has a confining phase for certain values of the coupling constant and hence we expect chiral symmetry breaking to occur in this theory as well.

In the case of massless fermions, i.e. $M = 0$, the QED-action (2.1) is also invariant under so-called chiral transformations

$$\psi(x) \to e^{i\,\epsilon\,\gamma_5}\psi(x), \qquad \bar{\psi} \to \bar{\psi}(x)e^{i\,\epsilon\,\gamma_5}. \tag{2.9}$$

The suitable operator describing chiral symmetry is γ_5 and is defined in the following way:

$$\gamma_5 = \gamma_0\gamma_1\gamma_2\gamma_3. \tag{2.10}$$

When working with Euclidean coordinates γ_5 has to be multiplied by i. Furthermore γ_5 is hermitean and has the following two properties:

$$\gamma_5\gamma_\mu = -\gamma_\mu\gamma_5 \quad \text{and} \quad (\gamma_5)^2 = 1. \tag{2.11}$$

At this stage one can define so-called projection operators out of the γ_5

$$\mathcal{P}_\pm = \frac{1}{2}(1 \pm \gamma_5). \tag{2.12}$$

Applied to a field ψ, $\mathcal{P}_\pm$ projects out the components $\psi_\pm = \mathcal{P}_\pm\psi$, which are eigenstates of γ_5 and take on the values ± 1.

An indicator of spontaneous chiral symmetry breaking is the generation of a chiral condensate, meaning

$$\langle\bar{\psi}\,\psi\rangle \neq 0 \tag{2.13}$$

even for massless fermions. This is indeed observed in the confining phase of QED.

2.1.2 Euclidean formulation

Further calculations will be done in Euclidean space-time, meaning that we choose the time coordinate to be purely imaginary

$$x^0 = -ix^4, \qquad \text{with} \quad x^4 \in \mathbf{R}. \tag{2.14}$$

This is the so-called Wick rotation. In order that Euclidean correlation functions can be transformed back to Minkowski space-time they have to obey

a positivity condition, called reflection positivity (see e.g. [5]). Performing the Wick rotation we end up with a Euclidean metric $\delta_{\mu\nu}$ for the coordinates $x^1, \dots x^4$

$$x \cdot y \equiv \delta_{\mu\nu} x^\mu y^\nu = x^1 y^1 + x^2 y^2 + x^3 y^3 + x^4 y^4 = -x * y. \tag{2.15}$$

Here the dot (star) denotes the scalar product in Euclidean (Minkowski) space-time. Note, that the covariant and contravariant components of a Euclidean vector are identical. Choosing the γ-matrices in a hermitean way $\gamma_4^E = \gamma^0$ and $\gamma_i^E = -i\gamma^i$ we end up with the Euclidean QED action

$$S^E_{\rm QED} = S^E_{\rm F} + S^E_{\rm G} \tag{2.16}$$

where

$$S^E_{\rm G} = \frac{1}{4e^2} \int d^4x \; F_{\mu\nu} F_{\mu\nu}, \tag{2.17}$$

$$S^E_{\rm F} = \int d^4x \; \bar{\psi}(x)(\gamma_\mu \mathcal{D}_\mu + M)\psi(x). \tag{2.18}$$

Hence the action (2.1) goes over into $iS^E_{\rm QED}$. Note, that in Euclidean coordinates γ_5 has to be multiplied by i.

2.2 Path integral formalism

Path integrals were first proposed by R. Feynman [6] and have many advantages compared to the operator formalism when quantizing fields [4]. Almost every book on quantum field theory devotes some pages to path integrals (see for example [3, 4, 7, 8]) and therefore I will not go too deep into the details.

2.2.1 The path integral in quantum mechanics

The quantum mechanical transition amplitude is given by

$$\langle x', t' | x, t \rangle = \langle x' | e^{-iH(t'-t)} | x \rangle. \tag{2.19}$$

Dividing the time interval t'- t into n equal parts and inserting (n-1) complete sets of eigenstates one arrives at

$$\langle x', t' | x, t \rangle = \int dx_1 \dots dx_{n-1} \langle x' | e^{-iH(t'-t_{n-1})} | x_{n-1} \rangle \dots \langle x_1 | e^{-iH(t_1-t)} | x \rangle. \tag{2.20}$$

To further specify the Hamilton we make use of the Baker-Hausdorff formula and by means of a Fourier transformation we arrive at

$$\langle x_{k+1}|e^{-iH(t'-t)}|x_k\rangle = \int \frac{dx_1\dots dx_{n-1}}{(\frac{2\pi i\Delta t}{m})^{n/2}}\exp\Big(i\sum_{k=0}^{n-1}\Delta t\{\frac{m}{2}(\frac{x_{k+1}-x_k}{\Delta t})^2 - V(x_k)\}\Big). \tag{2.21}$$

Let $n \to \infty$ and the exponent becomes

$$\int_0^T dt\,\Big\{\frac{m}{2}(\frac{dx}{dt})^2 - V(x)\Big\} = \int_0^T dt\,L(x,\dot{x}) \equiv S. \tag{2.22}$$

This is the classical action for a particle moving along a path x(t) from x to x'. The integration is over all possible paths x(t) and hence the measure of integration can be written as

$$\lim_{n\to\infty}(\frac{m}{2\pi i\Delta t})^{n/2}dx_1\dots dx_{n-1} = \mathcal{D}x. \tag{2.23}$$

Now we have arrived at the path integral representation of the quantum mechanical amplitude

$$\langle x'|e^{-iH(t'-t)}|x\rangle = \int \mathcal{D}x e^{iS}. \tag{2.24}$$

2.2.2 Functional integrals

As we want to do quantum field theory we have to translate the representation of quantum mechanics to path integrals. In field theory one has to deal with vacuum expectation values of field operators, called the Green's functions. From these various correlation functions can be obtained.

The formalism developed in the last chapter holds for any quantum system, so it should hold for a quantum field theory (QFT). The exact derivation can be found in any field theory book (see e.g. [3,4,8,9]) and hence I will give just the 'translation rules' when going from quantum mechanics to quantum field theory without deriving them exactly:

$$x_i(t) \longleftrightarrow \phi(\vec{x},t)$$

$$i \longleftrightarrow \vec{x}$$

$$\prod_{t,i} dx_i(t) \longleftrightarrow \prod_d d\phi(\vec{x},t) \equiv \mathcal{D}\phi$$

$$S = \int dt\,L \longleftrightarrow S = \int dt\,d^3x\,\mathcal{L}$$

Euclidean field theory	**Classical statistical mechanics**
Action S_{E}	Hamiltonian H
Units of action $\hbar$	Units of energy $\beta = \frac{1}{kT}$
$e^{-S_{\mathrm{E}}/\hbar}$	$e^{-\beta H}$
$\int \mathcal{D}\phi\, e^{-S_{\mathrm{E}}/\hbar}$	Partition function $\sum_{\mathrm{conf.}} e^{-\beta H}$
Vacuum energy	Free energy
Vacuum expectation value $\langle 0\|\mathcal{O}\|0\rangle$	Canonical ensemble average $\langle \mathcal{O} \rangle$
Time ordered products	Ordinary products
Green's functions	Correlation functions
Mass M	Correlation length $\xi = 1/M$
Regularization: cutoff Λ	Lattice spacing a
Renormalization: $\Lambda \to \infty$	Continuum limit $a \to 0$

Table 2.1: The table shows the equivalence between a Euclidean field theory and classical statistical mechanics.

Now we can write down the Green's functions in terms of *functional integrals*

$$\langle 0|\phi(x_1)\phi(x_2)\dots\phi(x_n)|0\rangle = \frac{1}{Z}\int \mathcal{D}\phi\ \phi(x_1)\phi(x_2)\dots\phi(x_n)e^{iS} \tag{2.25}$$

$$Z = \int \mathcal{D}\phi\ e^{iS} \tag{2.26}$$

Note that the integrand is oscillating due to the imaginary exponent. But again changing from Minkowski to Euclidean space-time will result in

$$Z = \int \mathcal{D}\phi\ e^{-S_{\mathrm{E}}}, \tag{2.27}$$

with S_{E} being the Euclidean action. The exponent has become real now and it is a reasonable statistical weight for the fluctuations of ϕ.

As mentioned in the introduction there is a close connection between Minkowski and Euclidean Field theory and statistical mechanics. This is most transparent if the field theory is quantized using the Feynman path integral approach. Table (2.1) shows the equivalences between classical statistical mechanics and Euclidean field theory. This will be seen even more clearly when we are introducing the lattice as a regularization scheme.

From now on the Euclidean formulation will be used and unless explicitly stated any labeling refering to this shall be dropped.

2.3 The Landau pole problem

As mentioned in the introduction, an apparent mathematical inconsistency in QED is the existence of the so-called Landau pole. It appears in the perturbative behavior of the renormalized coupling constant as a function of the cut-off parameter.
The Callan-Symanzik β-function is defined as

$$\beta(\alpha) = -\Lambda\Big(\frac{\partial\alpha}{\partial\Lambda}\Big)_{e,m_R}, \tag{2.28}$$

where α is the renormalized fine structure constant, Λ the cut-off and the derivative is to be taken at fixed bare coupling e and renormalized m_R. The dependence of α on Λ is obtained from the differential equation

$$\frac{d\alpha}{d\ln\Lambda} = -\beta(\alpha) \tag{2.29}$$

and we obtain for the one-loop approximation to the β-function with only one fermion species

$$\alpha\Big(\frac{\Lambda}{m_R}\Big) = \frac{\alpha_0}{1+\alpha_0\beta_1\ln(\Lambda/m_R)}, \quad \beta_1 = \frac{2}{3\pi}, \quad \alpha_0 = \frac{e^2}{4\pi}. \tag{2.30}$$

Trying to send Λ to infinity while keeping α_0 fixed, α approaches zero and the theory would be trivial. Two-loop contributions would not change the result qualitatively.

Now consider the renormalized coupling $e_R^2 = 4\pi\alpha$ instead of α. The β-function now determines the change of e_R^2 as a function of μ, the renormalization scale. The differential equation is obtained to be

$$\frac{de_R^2(\mu)}{d\log\mu} = \beta_{e^2}(e_R^2(\mu)), \quad \beta_{e^2} = 4\pi\beta \tag{2.31}$$

and in the one-loop approximation we find

$$e_R^2(\mu) = \frac{e_R^2(\mu_0)}{1 - e_R^2(\mu_0)(\beta_1/4\pi)\ln(\mu/\mu_0)}. \tag{2.32}$$

$e_R^2(\mu)$ has a pole at the scale

$$\mu_{\text{Landau}} = \mu_0\exp\Big(\frac{4\pi}{\beta_1 e_R^2(\mu_0)}\Big), \tag{2.33}$$

if it is equal $e_R^2(\mu_0)$ at the scale μ_0. The position of the Landau pole is changed by the two-loop contribution to

$$\mu_{\text{Landau}} = \mu_0 \Big(\frac{\beta_2 e_R^2(\mu_0)}{4\pi\beta_1} \Big)^{\frac{\beta_2}{\beta_1^2}} \exp\Big(\frac{4\pi}{\beta_1 e_R^2(\mu_0)} \Big) \big(1 + \mathcal{O}(e_R^2(\mu_0)) \big), \tag{2.34}$$

and substituting $e_R^2(\mu_0) = 4\pi/137$ we end up with a very high scale, far away from any reasonable scale. This mathematical inconsistency can be resolved if the full β-function has the zero at $e_R^2 = e_*^2$, an ultra-violet stable fixed point. This means that the solution of (2.31) for $e_R^2(\mu)$ always tends towards e_*^2 as μ goes to infinity. The zero of (2.29) implies that we can tune α_0 near $\alpha_{0*} = e_*^2/4\pi$ in a way such that for $\Lambda \to \infty$, α gets an arbitrary finite value. Thus, if such a fixed point exists, the continuum limit is non-trivial.

The zero of the β-function may be associated with a QED phase transition in the bare parameter space. At this critical point e_*^2, which is in the strong coupling regime, the chiral symmetry of the massless theory is spontaneously broken and the chiral condensate $\langle \bar{\psi}\psi \rangle$ becomes non-zero. Later on the phase structure of QED is discussed in more detail.

To find a solution to the Landau pole problem, QED has to be formulated in a non-perturbative way. Thus, it was self-evident to investigate the problem on the lattice (see e.g. [10, 11]).

It should be mentioned that QED is not the only theory showing the Landau pole problem. Every theory which is not asymptotically free suffers from this problem.

Herewith the recapitulation of the basics of continuum quantum electrodynamics is completed and it's high time to continue with the introduction of the space-time lattice.

Chapter 3

The space-time lattice

When doing QFT one has to deal with several types of divergencies. Regularization is an important tool to get rid of them. This in turn means a kind of cut-off for some parameters. Up to the present several possibilities are known to do so.

In 1974 K. Wilson [12] came up with the idea to introduce a space-time lattice and put a field theory on it. The first question physicists were interested in was whether QCD is able to account for quark confinement. The lattice allows one to use non-perturbative techniques and to keep gauge invariance; it therefore provides a way to make predictions in the low energy range using numerical methods.

The next chapters will explain the main concepts of lattice gauge theory with the focus on the $U(1)$ gauge group.

3.1 Lattice regularization

In the quantum mechanical case the path integral is defined as a limit of a finite-dimensional integral resulting from a discretization of time. This will now be carried over to field theory by considering the functional integral as a limit of a well-defined integral over discretized Euclidean space-time.

We begin with introducing a hyper-cubical lattice

$$\Lambda = a\boldsymbol{Z}^4 = \{x | x_\mu / a \in \boldsymbol{Z}\} \tag{3.1}$$

where a is the lattice constant and $\mu = 1, \ldots, 4$. A field $\phi(x)$ is defined on the lattice points $x \in \Lambda$. Carrying over some analogies from the continuous case we set

$$(f, g) = \sum_x a^4 f(x) g(x) \tag{3.2}$$

and define the lattice forward and backward derivative by

$$\triangle_\mu^f f(x) = \frac{1}{a}(f(x + a\hat{\mu}) - f(x))$$
$$\triangle_\mu^b g(x) = \frac{1}{a}(g(x) - g(x - a\hat{\mu})) \tag{3.3}$$

where $\hat{\mu}$ is the unit vector in the direction μ. We have

$$(\triangle_\mu^f f, g) = -(f, \triangle_\mu^b g) \tag{3.4}$$

This implies

$$(\triangle_\mu^f f, \triangle_\mu^f f) = -(f, \triangle_\mu^b \triangle_\mu^f f) \equiv (f, \Box f) \tag{3.5}$$

where the lattice d'Alembert operator $\Box = -\triangle_\mu^b \triangle_\mu^f$ acts on functions as

$$\Box f(x) = \sum_{\mu=1}^{4} \frac{1}{a^2}(2f(x) - f(x + a\hat{\mu}) - f(x - a\hat{\mu})) \quad . \tag{3.6}$$

On such a lattice the fields $\bar{\psi}$ and ψ are located on the sites, i.e. $\bar{\psi}(x)$ and $\psi(x)$.

3.2 Gauge field discretization

The gauge fields are described by variables connecting different lattice points with finite separation a. They point and act in certain directions and hence they are provided with a vector index μ. The local gauge invariance from the continuum theory (2.7) has to be reflected by the transformation properties of the lattice equivalent of the gauge field. Therefore we introduce so-called parallel transporters. They are obtained from taking the path ordered exponentials of the gauge field. Such a parallel transporter points from a lattice point x in a certain direction μ and is called *link variable*

$$U_\mu(x) = e^{i\,e\,a A_\mu(x)}. \tag{3.7}$$

The link variables are elements of the gauge group $U(1)$ and transform under local $U(1)$ gauge transformations as

$$U_\mu(x) \to \Lambda(x) U_\mu(x) \Lambda^{-1}(x + a\hat{\mu}). \tag{3.8}$$

The link variable has the property

$$U_{_\mu}(x) = U_\mu^\dagger(x - a\hat{\mu}) \tag{3.9}$$

Figure 3.1: Graphical representation of link variables.

and is therefore a directed quantity.

Unfortunately the lattice regularization scheme breaks the rotational or Lorentz-frame independence. But in the continuum limit, as $a \to 0$ all these symmetries are restored.

The next step now will be to find gauge invariant quantities in terms of these link variables.

In principle it is possible to consider the straightforwardly discretized version of the gauge action (2.17). In this case the vector potential $A_\mu(x)$ takes on values in the interval $(-\infty, +\infty)$ and we are talking about non-compact lattice QED. This theory can be used to study the Landau pole problem (see for example [10, 11]).

Nothing forbids us to restrict the link variables to the interval $(-\pi, +\pi]$. The exponent can be seen as a phase, giving the same values for integer multiples of 2π. These link variables are called compact link variables (3.7) and in this case we are talking about compact lattice QED. For more details on compactifying QED the reader is refered to [12] or promised to later chapters.

The simplest way to obtain a gauge invariant variable is to consider the path-ordered product of such link variables around a closed path

$$U_{\mathrm{P}} = U_{\mu,\nu}(x) \equiv U_\mu(x) U_\nu(x + a\hat{\mu}) U_\mu^\dagger(x + a\hat{\nu}) U_\nu^\dagger(x). \tag{3.10}$$

where the hat on the μ and ν denotes the unit vector in the particular direction. U_p is called plaquette variable and is visualized in Figure 3.2.

From this quantity the so-called Wilson gauge action or plaquette action can be constructed

$$S_{\mathrm{W}} = S_{\mathrm{P}}[U_{\mathrm{P}}] = \beta \sum_{x,\mu>\nu} (1 - \mathrm{Re} U_{\mathrm{P}}(x)), \tag{3.11}$$

where $\beta = 1/e^2$ is the inverse squared bare coupling parameter. This can be seen if we take a closer look at the plaquette action in the continuum limit. Therefore we use (2.5) and

$$a\, \partial_\mu A_\nu(x) = A_\nu(x + \hat{\mu}) - A_\nu(x) + \mathcal{O}(a^2). \tag{3.12}$$

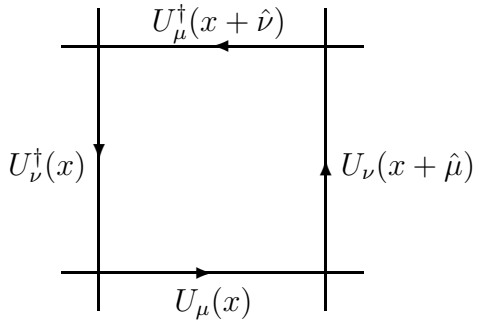

Figure 3.2: The simplest gauge invariant object on the lattice: a closed loop, called the Wilson loop.

Then we take the limit $a \to 0$ and obtain for the plaquette action

$$S = -\frac{\beta}{4} \sum_x a^4 F_{\mu\nu}(x) F_{\mu\nu}(x) + \mathcal{O}(a^2). \tag{3.13}$$

We immediately see the connection between the electric charge e in the continuum limit and the parameter β in (3.11)

$$\beta = \frac{1}{e^2}. \tag{3.14}$$

By rescaling the gauge fields A_μ we can get rid of any explicit factor of a. Therefore we can equally well put $a = 1$, i.e. use dimensionless quantities.

Such a discretization scheme is in a way arbitrary. But from universality it follows that we can manipulate the behavior of the lattice theory by adding terms which vanish as $a \to 0$ but do not alter the physical properties in the continuum limit.

3.3 Fermions on the lattice

The next step will consist of a discretization of the fermion part of the action (2.18). Actually we are left with the problem of finding a formulation for the derivative of the continuum Dirac operator on the lattice. This turns out to be quite a difficult task. Furthermore we demand the Dirac operator to have as many continuum properties as possible. This includes the correct behavior under gauge transformations as well as the invariance of the action

under charge conjugation, parity, rotations and translations. In addition the Dirac operator is required to be γ_5-hermitean, i.e. $\mathcal{D}\gamma_5 = \gamma_5\mathcal{D}^\dagger$.

The problems arising from the discretization (the occurrence of so-called *doublers*) of (2.18) are discussed in the next section 3.3.1. A first solution of this dilemma is provided by the Wilson fermions, which are subject of section 3.3.2. Other ways of improving the continuum limit of fermions are well-known and are mentioned afterwards in a short way. A major disadvantage of these solutions is that they explicitly break chiral symmetry. The best improvement is obtained from operators, which obey the so-called Ginparg-Wilson equation [13]. More about these operators is discussed in chapter 4.

3.3.1 The naive discretization

We begin by considering the Euclidean Dirac equation

$$S_{\mathrm{F}}^E = \int d^4x \bar{\psi}(x)(\gamma_\mu^E \partial_\mu + M)\psi(x), \tag{3.15}$$

where the Euclidean γ-matrices γ_μ^E satisfy the algebra

$$\{\gamma_\mu^E, \gamma_\nu^E\} = 2\delta_{\mu\nu}.$$

From now on we will use the Euclidean γ-matrices and the labels reminding of this will be dropped again. The fields ψ and $\bar{\psi}$ are four-component spinor fields and will be labeled by Greek indices.

Let us begin with putting the fields on the space-time lattice. The fields ψ and $\bar{\psi}$ then live on the lattice sites n which are separated by the lattice spacing a. To write the action in form of dimensionless lattice variables (denoted with a "hat") we have to scale M, ψ and $\bar{\psi}$. This can be achieved by making the replacements

$$\begin{aligned} M &\to \tfrac{1}{a}\hat{M}, \\ \psi_\alpha(x) &\to \frac{1}{a^{3/2}}\hat{\psi}_\alpha(n), \\ \bar{\psi}_\alpha(x) &\to \tfrac{1}{a^{3/2}}\bar{\hat{\psi}}^\alpha(n), \\ \partial_\mu\psi(x) &\to \tfrac{1}{a^{5/2}}\hat{\partial}_\mu\hat{\psi}(n), \end{aligned} \tag{3.16}$$

and $\hat{\partial}_\mu$ is the antihermitean lattice derivative defined by

$$\hat{\partial}_\mu \hat{\psi}_\alpha(n) = \frac{1}{2}[\hat{\psi}_\alpha(n+\hat{\mu}) - \hat{\psi}_\alpha(n-\hat{\mu}] \quad . \tag{3.17}$$

The lattice version of (2.18) now reads

$$S_F = \sum_{n,m,\alpha,\beta} \bar{\hat{\psi}}_\alpha(n) K_{\alpha\beta}(n,m) \hat{\psi}_\beta(n), \tag{3.18}$$

where

$$K_{\alpha\beta}(n,m) = \sum_\mu \frac{1}{2}(\gamma_\mu)_{\alpha,\beta}[\delta_{m,n+\hat{\mu}} - \delta_{m,n-\hat{\mu}}] + \hat{M}\delta_{mn}\delta_{\alpha\beta}. \tag{3.19}$$

The correlation function

$$\langle \hat{\psi}_\alpha(n) \ldots \bar{\hat{\psi}}_\beta(m) \ldots \rangle = \frac{\int D\bar{\hat{\psi}} D\hat{\psi}\, (\hat{\psi}_\alpha(n) \ldots \bar{\hat{\psi}}_\beta(m) \ldots) e^{-S_{\rm F}}}{\int D\bar{\hat{\psi}} D\hat{\psi} e^{-S_{\rm F}}}, \tag{3.20}$$

with the integration measure defined by

$$D\bar{\hat{\psi}} D\hat{\psi} = \prod_{n,\alpha} d\bar{\hat{\psi}}_\alpha(n) \prod_{m,\beta} d\hat{\psi}_\beta(m), \tag{3.21}$$

can now be obtained by differentiating the generating functional

$$Z[\eta,\hat{\eta}] = \int D\bar{\hat{\psi}} D\hat{\psi}\, e^{-S_{\rm F} + \sum_{n,\alpha}[\bar{\eta}_\alpha(n)\hat{\psi}_\alpha(n) + \bar{\hat{\psi}}_\alpha(n)\eta_\alpha(n)]} \tag{3.22}$$

with respect to the Grassmann sources (see Appendix A.1). The integral (3.22) can be performed, giving (see Appendix A.1)

$$Z[\eta,\bar{\eta}] = (\det K) e^{\sum_{n,m,\alpha,\beta} \bar{\eta}_\alpha(n) K^{-1}_{\alpha\beta}(n,m) \eta_\beta(m)}. \tag{3.23}$$

The simplest case we can consider is the two-point function, which is given by

$$\langle \hat{\psi}_\alpha(n)\, \bar{\hat{\psi}}_\beta(m) \rangle = K^{-1}_{\alpha\beta}(n,m). \tag{3.24}$$

At this point let us take a look at the continuum limit of (3.24), which corresponds to the physical correlation function

$$\langle \psi_\alpha(x)\, \bar{\psi}_\beta(y) \rangle = \lim_{a\to 0} \frac{1}{a^3}\, G_{\alpha\beta}\, (\frac{x}{a}, \frac{y}{a}, Ma), \tag{3.25}$$

where $G_{\alpha\beta}(n,m,\hat{M}) \equiv K^{-1}_{\alpha\beta}(n,m)$.

Let us switch to momentum space for a moment. On an infinite volume lattice the Dirac δ-function δ_{nm} is given by

$$\delta_{nm} = \int_{-\pi}^{\pi} \frac{d^4\hat{p}}{(2\pi)^4}\, e^{i\hat{p}\,(n-m)}, \tag{3.26}$$

whereby the hat on $\hat{p} = ap$ again denotes the non-dimensionality of these variables. Using the Fourier representation of the delta function (3.26) in (3.19) and we obtain

$$K_{\alpha\beta}(n,m) = \int_{-\pi}^{\pi} \frac{d^4\hat{p}}{(2\pi)^4} \tilde{K}_{\alpha\beta}(\hat{p})\, e^{i\hat{k}\,(n-m)} \tag{3.27}$$

where

$$\tilde{K}_{\alpha\beta}(\hat{p}) = -i \sum_{\mu} (\gamma_\mu)_{\alpha\beta} \sin(\hat{p}_\mu) + \hat{M}\delta_{\alpha\beta}. \tag{3.28}$$

Note that the integration in (3.27) is restricted to the interval $[-\pi, \pi]$. Now let us make the ansatz

$$K^{-1}_{\alpha\beta}(n,m) = \int_{-\pi}^{\pi} \frac{d^4\hat{p}}{(2\pi)^4}\, G_{\alpha\beta}(\hat{p})\, e^{i\hat{k}\,(n-m)}$$

where $G_{\alpha\beta}(\hat{p})$ is the Green's function in discretized momentum space and execute the summation over α and β to obtain

$$K^{-1}_{\alpha\beta}(n,m) = \langle \psi_\alpha(n)\, \bar{\psi}_\beta(m) \rangle = \int_{-\pi}^{\pi} \frac{d^4\hat{p}}{(2\pi)^4} \frac{[-i\sum \gamma_\mu \hat{p}_\mu + \hat{M}]_{\alpha\beta}}{\sum_\mu \hat{p}_\mu^2 + \hat{M}^2} e^{i\hat{p}\,(n-m)}. \tag{3.29}$$

The most obvious thing now would be to rescale $\hat{\psi}$ and $\hat{M}$ and to take the limit $a \to 0$, keeping the quantities ψ, M, $x = na$ and $y = ma$ fixed. But this means that we must know which quantities are to be held fixed. However, in our naive procedure we arrive at the correct continuum limit (3.25). After a trivial change in the integration variables we find that

$$\langle \psi_\alpha(x)\, \bar{\psi}_\beta(y) \rangle = \lim_{a\to 0} \int_{-\pi/a}^{\pi/a} \frac{d^4p}{(2\pi)^4} \frac{[-i\sum \gamma_\mu \tilde{p}_\mu + M]_{\alpha\beta}}{\sum_\mu \tilde{p}_\mu^2 + M^2}\, e^{ip\,(x-y)}, \tag{3.30}$$

where $\tilde{p}_\mu$ is given by

$$\tilde{p}_\mu = \frac{1}{a} \sin(p_\mu a). \tag{3.31}$$

The integral will be dominated by momenta which are small compared to the inverse lattice spacing and we may set $\tilde{p}_\mu \to p_\mu + \mathcal{O}(a^2)$. Then the above integral would reduce to the well-known 2-point function in the limit $a \to 0$.

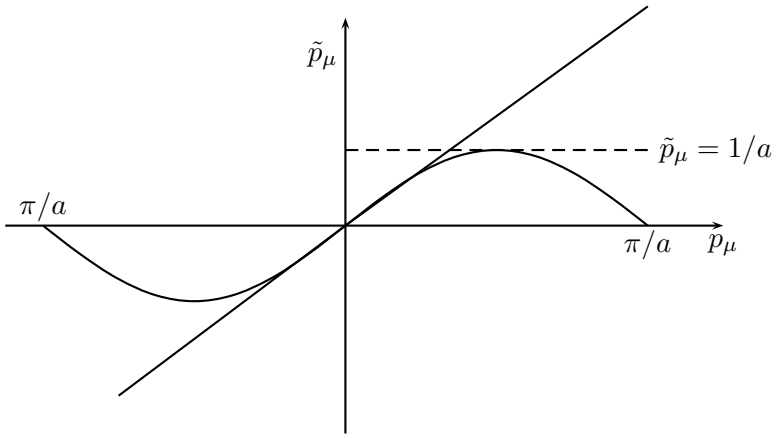

Figure 3.3: Plot of $\sin(p_\mu a)/a$ versus a in the Brillouin zone to display the fermion doubling problem.

This is still not entirely satisfactory since $\sin(p_\mu + \pi) = \sin(p_\mu)$ all give the same result $\tilde{p}^2_\mu(p_\mu) = \tilde{p}^2_\mu(p_\mu + \pi)$. Thus, within the Brillouin zone the sine function (3.31) has 16 zeros! This is the origin of the so-called *fermion doubling problem*. Inside half of the Brillouin zone in each direction, near the continuum limit, the deviation from the straight line behavior occurs only for large momenta where both, p_μ and $\tilde{p}_\mu$, are of order $1/a$. What actually is destroying the correct limit are the zeros of the sine function at the edges of the Brillouin zone. The result is that there are sixteen regions of integrations, where p_μ takes a finite value in the limit $a \to 0$. Fifteen of these involve high momentum excitations of the order π/a, which give rise to a momentum distribution having the form of a single particle propagator. Hence these lattice theory actually contains sixteen species of fermions. In d dimensions the number would be 2^d, meaning it doubles for each additional dimension. The inclusion of the gauge fields does not solve the doubling problem either.

The chiral transformations, defined in (2.9) are realized on the lattice if $\gamma_5 M + M\gamma_5 = 0$. The naive lattice action satisfies the hermiticity property $\gamma_5 M \gamma_5 = M^\dagger$. Thus the Euclidean lattice action has to be antihermitean in the massless limit for chiral symmetry to hold.

The question now is under which general conditions a lattice theory exhibits doublers. The answer is given by the Nielsen-Ninomiya theorem [14]. Consider a generalized action such that $S^{-1}(p, M = 0) = iF(p)$. Then the corresponding lattice theory will have doublers, if:

- $F(p)$ has a periode in momentum space of $\frac{2\pi}{a}$

- the momenta on the lattice are continuous in the range $\{0, 2\pi\}$.
- $F(p)$ is continuous in the momentum space
- $F(p) \rightarrow p_\mu \gamma_\mu$ for small momenta and coincides with the continuum theory in the limit $a \rightarrow 0$.
- the action possesses chiral symmetry.

We have seen now that our naive ansatz of discretizing the fermion fields is accompanied by the occurrence of unwanted doublers. But fortunately there are several possibilities to obtain the correct continuum limit, i.e. eliminate the extra fermion species. They all have in common that one has to pay the price that chiral symmetry on the lattice is explicitly broken. An alternative way, neither without any problems, to retain a chirally symmetric formulation (with only a local breaking of chiral symmetry) is provided by the Ginsparg-Wilson relation [13] and is subject of later chapters.

3.3.2 Wilson fermions

This is the most popular way dealing with the doubling problem and was first elaborated by Wilson in 1974. As already mentioned above there is some freedom to add terms to the naive action in a way that the zeros of the denominator at the edges of the Brillouin zone are lifted by an amount proportional to the inverse lattice spacing. These terms of course have to vanish in the continuum limit. A good candidate would be a second derivative:

$$S_F^{(W)} = S_F - \frac{r}{2} \sum_n \bar{\hat{\psi}}(n) \hat{\Box} \hat{\psi}(n), \tag{3.32}$$

where $\hat{\Box}$ is the four-dimensional lattice Laplacian

$$\hat{\Box} \hat{\psi}(n) = \sum_\mu \left[2\hat{\psi}(n) - \hat{\psi}(n + \hat{\mu}) - \hat{\psi}(n - \hat{\mu}) \right].$$

Here r is called the Wilson parameter, which is expected to be irrelevant at the renormalization or finetuning of lattice observables. Therefore and also for convenience we may set it later on equal to 1. By setting $\hat{\psi} = a^{3/2}\psi$ and $\hat{\Box} = a^2 \Box$, we see that the Wilson term vanishes with $\mathcal{O}(a)$ in the naive continuum limit. Inserting for $\hat{\Box}\hat{\psi}(n)$ one obtains for the Wilson fermion action

$$S_F^{(W)} = \sum_{n,m} \bar{\hat{\psi}}(n) K_{nm}^{(W)} \hat{\psi}(m), \tag{3.33}$$

with

$$K^{(W)}_{nm} = (\hat{M} + 4r)\delta_{nm} - \frac{1}{2}\sum_{\mu n}[(r-\gamma_\mu)\delta_{m,n+\hat{\mu}} + (r+\gamma_\mu)\delta_{m,n-\hat{\mu}}] \tag{3.34}$$

For $r \neq 0$ chiral symmetry is explicitely broken, even for $\hat{M} \to 0$. The Wilson action now leads to the following two-point function

$$\langle \psi(x)\hat{\psi}(y)\rangle = \lim_{a\to 0}\int_{-\pi/a}^{\pi/a} \frac{d^4p}{(2\pi)^4}\frac{[-i\sum\gamma_\mu\tilde{p}_\mu + M(p)]}{\sum_\mu \tilde{p}^2_\mu + M(p)^2}e^{ip(x-y)}, \tag{3.35}$$

with

$$M(p) = M + \frac{2r}{a}\sum_\mu \sin^2(p_\mu\frac{a}{2}). \tag{3.36}$$

For any fixed value of p_μ, $M(p)$ approaches M as $a \to 0$. But near the boundaries of the Brillouin zone $M(p)$ diverges as a approaches zero.

The interaction matrix is often expressed in a manner containing the links

$$K^{(W)}_{nm}[U] = \delta_{nm} - \kappa\sum_{\mu>0}[(r-\gamma_\mu)U_\mu(n)\delta_{n+\hat{\mu},m} + (r+\gamma_\mu)U^\dagger_\mu(n-\hat{\mu})\delta_{n-\hat{\mu},m}] \tag{3.37}$$

so that (3.33) becomes

$$S^{(W)}_F = \sum_{n,m}\bar{\hat{\psi}}(n)K^{(W)}_{nm}[U]\hat{\psi}(m), \tag{3.38}$$

with the so-called hopping parameter κ

$$\kappa = \frac{1}{2\hat{M} + 2dr} \tag{3.39}$$

and rescaled fermion fields by the coefficient $\sqrt{2\kappa/a^3}$. Here d is the number of dimensions. Figuratively the local term tries to keep the fermion at the same site while the non-local term makes the fermion hop to the nearest neighbour site with strength κ. The fermion matrix (3.37) exhibits the following properties

- there is a remnant of discrete symmetries: $\gamma_5 K^{(W)\dagger}_{nm}[U]\gamma_5 = K^{(W)}_{nm}[U]$, i.e. it is γ_5-hermitean
- $\hat{\bar{\psi}}(n)\Lambda(n)K^{(W)}_{nm}[U]\Lambda^\dagger(m)\hat{\psi}(m) = \hat{\bar{\psi}}(n)K^{(W)}_{nm}[U]\hat{\psi}(m)$, i.e. covariance under the gauge transformations (3.8).

The adjoint $K^{(W)\dagger}_{nm}$ is taken with respect to the coordinate and spinor indices.

From (3.39) we see that for the free theory in 4 dimensions the fermion mass is given in terms of the lattice parameters κ and r as

$$ma = \frac{1}{2\kappa} - 4r = \frac{1}{2\kappa} - \frac{1}{2\kappa_c}, \tag{3.40}$$

with $m = 0$ at $\kappa = \kappa_c = 1/8r$. In the interacting case we perpetuate (3.40) but demand κ_c depending on the lattice spacing a. The renormalization of κ_c implies that the fermion mass has both multiplicative and additive renormalizations and follows from the explicit breaking of chiral symmetry by the term proportional to r in (3.37). Thus, Wilson's solution for the fermion doubling problem is accompanied with the unwanted effect of explicitly breaking chiral symmetry.

3.3.3 More Dirac operators

The so-called *staggered fermion* formulation will be mentioned here just for the sake of completeness without working out the details. For details the reader is refered to [15, 16].

To prevent the function (3.31) from vanishing at the corners of the BZ we try to eliminate the unwanted fermion modes by reducing the BZ, i.e. doubling the effective lattice spacing. Therefore in principle we have to distribute the fermionic degrees of freedom in such a way that the effective lattice spacing for each type of Grassmann variable is twice the fundamental lattice spacing and the action has to reduce to the continuum form in the continuum limit. The doublers are transformed to $2^{d/2}$ fermion flavours by means of the spin diagonalization of the naive action. This formulation is invariant under global chiral symmetry transformations (2.9). However, in 4 dimensional space-time the staggered fermion model contains 4 mass degenerate flavours.

Yet another method to improve the fermion part of the action in the continuum limit $a \to 0$ comes under the name of *clover improvement* (for details see e.g. [16–18]). Sheikholeslami and Wohlert proposed to add another term to the fermionic Wilson action

$$S_W + c_{\rm SW}\frac{i}{4}\bar{\psi}(x)\sigma_{\mu\nu}F_{\mu\nu}(x)\psi(x).$$

$\sigma_{\mu\nu}$ are commutators of Dirac matrices (A.14) and $F_{\mu\nu}$ the discretized field strength tensor.

This completes the discussion of Dirac operators breaking chiral symmetry and we may now write down the full QED action for e.g. Wilson fermions:

$$\begin{aligned} S_{\mathrm{QED}}[U,\psi,\bar{\psi}] &= \beta\sum_P[1-\frac{1}{2}(U_{\mathrm{P}}-U_{\mathrm{P}}^\dagger)] \\ +(\hat{M}+4r)\sum_n\bar{\psi}(n)\psi(n) &- \frac{1}{2}\sum_{n,\mu}\big[\bar{\psi}(n)(r-\gamma_\mu)U_\mu(n)\psi(n+\hat{\mu}) \\ &+\bar{\psi}(n+\hat{\mu})(r+\gamma_\mu)U_\mu^\dagger(n)\psi(n)\big]. \end{aligned} \tag{3.41}$$

To calculate any correlation function of the fermionic as well as of the link variables, (3.41) has to be used in a path integral formulation. This is subject to the next section.

3.4 Observables on the lattice

The lattice QED action for Wilson fermions (3.41) consists of the pure gauge part (3.11) and the fermion part (3.38)

$$S_{\mathrm{QED}}[U,\bar{\psi},\psi] = S_{\mathrm{P}}[U] + S_{\mathrm{F}}^W[U,\bar{\psi},\psi]. \tag{3.42}$$

In order to extract measurable quantities we have to insert (3.42) into path integrals. The path integral will comprise integrations over all U_μ. These are elements of a unitary group and the integrations have to be performed over the whole group manifold, which in the present $U(1)$ case is parametrized by one real angular variable, restricted to the interval $[0, 2\pi)$. As the gauge invariance of the action should not be quashed during the integration process the integration measure must be gauge invariant as well and is given by

$$DU \equiv \prod_{n,\mu} d\phi_\mu(n). \tag{3.43}$$

Here I have used the parametrization $U_\mu(n) = e^{i\phi_\mu(n)}$. The integration measure (3.43) is called Haar measure (see e.g. [19]). Now we can compute correlation functions of the Dirac fields and link variables from the path integral expression

$$\langle\mathcal{O}\rangle = \frac{1}{Z}\int DU D\bar{\psi}D\psi\mathcal{O}[U,\bar{\psi},\psi]e^{-S_{\mathrm{QED}}[U,\bar{\psi},\psi]}, \tag{3.44}$$

with the partition function (or normalization constant)

$$Z = \int DU D\bar{\psi}D\psi\, e^{-S_{\mathrm{QED}}[U,\bar{\psi},\psi]}. \tag{3.45}$$

The fermion part of the action is a bilinear form in the Grassmann valued variables $\bar{\psi}$ and ψ. The fermionic fields can be integrated out analytically (see Appendix A.2). To this end we have to use the generating functional of the theory. In our case it is given by

$$W[U,\bar{\eta},\eta] = \frac{1}{Z}\int DU D\bar{\psi} D\psi \, e^{-S_{\mathrm{P}}[U]} \tag{3.46}$$
$$e^{-\sum_{n,m}\bar{\psi}_\alpha(n)K_{\alpha\beta}(n,m)\psi_\beta(m)+\sum_{n,\alpha}[\bar{\eta}_\alpha(n)\psi_\alpha(n)+\bar{\psi_\alpha}(n)\eta_\alpha(n)]},$$

where $K_{\alpha\beta}(n,m)$ is the lattice Dirac operator (3.19). Making use of the equations from Appendix A.2 we finally end up with

$$W[U,\bar{\eta},\eta] = \frac{1}{Z}\int DU \det K e^{-S_{\mathrm{P}}[U]} e^{\sum_{n,m,\alpha,\beta}\bar{\eta}_\alpha(n)K^{-1}_{\alpha\beta}(n,m)\eta_\beta(m)}. \tag{3.47}$$

With this expression fermionic fields appearing in the path integral can be transformed into propagators, which depend on the gauge field only. Expectation values can be obtained by differentiating (3.46) or (3.47) with respect to the Grassmann valued sources $\eta_\alpha(n)$ and $\bar{\eta}_\alpha(n)$.

It is not possible to calculate ensemble averages for products of Grassmann variables using statistical methods. But the fermionic contributions to the action are bilinear in the fermion fields ψ and $\bar{\psi}$ and hence we can perform the Grassmann integrals and rearrange the path integral expression for the euclidean correlation function into a statistical mechanical average with a new effective action. Unfortunately, this action (due to the determinant) depends in a non-local way on the bosonic fields to which the fermion fields are coupled. And it is this non-locality which makes computational evaluations of correlation functions so time consuming.

3.5 Renormalization on the lattice

The most important question in lattice theories is whether in the continuum limit the integrated theory corresponds to any theory like QED, QCD, etc. Or in other words, if there is a critical region in parameter space where correlation lengths diverge and one can remove the cutoff. The procedure is a variant of the renormalization group methods and is non-perturbative.

Suppose a lattice theory contains parameters Q_i. An example would be β in (3.41). Multiplying by suitable powers of the lattice constant a, all Q_i can be defined as dimensionless quantities $\hat{Q}_i = aQ_i$. Suppose further we must rely on a numerical calculation of (3.22) where the lattice spacing does not appear. Now we introduce the physical correlation lengths ξ_i. The

corresponding lattice quantity $\hat{\xi}_i$ will vary as a is changed. In the case $a \to 0$, $\hat{\xi}_i$ must diverge in order to keep the physical quantity ξ_i fixed. Dimensionless masses have the form

$$\hat{M}_i = \frac{1}{\hat{\xi}_i}, \tag{3.48}$$

leading to the following expression of e.g. the exponentially decaying two-point function with distance n between the two points in units of a:

$$\langle \phi_i(x)\phi_i(x + na\hat{\mu})\rangle \propto e^{-n/\hat{\xi}_i}. \tag{3.49}$$

Inserting in this expression ξ_i from (3.48), the typical behavior of the propagator for a particle with mass M_i is obtained. The divergence of $\hat{\xi}_i$ if $a \to 0$ means that the continuum limit is realized for $\hat{M}_i \to 0$ at a critical point of the theory. Thus, a fundamental requirement for the construction of a continuum limit is the existence of a continuous phase transition, i.e. the transition must be of second or higher order for some critical values Q_i^c.

Another important condition for the renormalizability of a lattice theory is the validity of a scaling behavior of the parameters approaching the critical point $Q_i \to Q_i^c$. Masses in lattice field theories usually have a scaling behavior of the type

$$\frac{1}{\hat{\xi}_i} = aM_i \simeq \alpha_i |Q_i - Q_i^c|^\nu. \qquad \nu > 0 \tag{3.50}$$

or in the case $Q_i^c = \infty$,

$$\frac{1}{\hat{\xi}_i} = aM_i \simeq \alpha_i e^{-b_i Q_i}, \qquad b > 0. \tag{3.51}$$

If one of the equations (3.50) and (3.51) holds, the limit $Q_i \to Q_i^c$ for masses can be performed resulting in

$$\frac{M_i}{M_1} = \frac{\alpha_i}{\alpha_1}. \tag{3.52}$$

This is a nice result since taking a value for M_1 from e.g. the experiment in GeV we easily obtain predictions for the other masses in the continuum limit. Additionally, by solving (3.50) and (3.51) for a information about the size of the lattice constant in $(\text{GeV})^{-1}$ in the vicinity of the critical point is obtained

$$a \simeq \frac{1}{M_1}\alpha_1 |Q - Q^c|^\nu \qquad a \simeq \frac{1}{M_1}\alpha_1 e^{-bQ}. \tag{3.53}$$

This result shows that any calculation, both practical and analytical, should be performed in the vicinity of the critical point.

Other physical quantities, like the coupling constant or the condensate, are treated in a similar way.

QCD has the nice property of being asymptotically free and hence the critical point is at $\beta^c = \infty$. The scaling behavior of (3.51) holds with a value of b known from renormalization group analysis. Thus quite reliable results have been obtained by extrapolating quantities into the limit $a \to 0$.

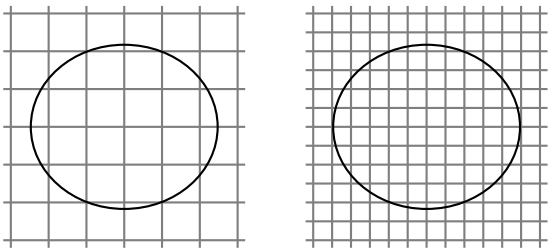

Figure 3.4: Tuning the lattice spacing a in order to keep physics the same.

To gain better insight into renormalization on the lattice the situation is depicted in Figure 3.4. Suppose the number of lattice points within the enclosing circle corresponds to a bare quantity living on the lattice, for example the mass $\hat{M}$. We want to hold the quantity M (represented by the circle) fixed by its physical value. As we make the lattice spacing finer and finer, more and more lattice points migrate into the circle to keep the volume (M) constant. Thus, if physics is to remain the same at all lattice spacings, the bare parameters of the theory must be tuned to a in a way depending on the dynamics of the theory.

3.6 The phase structure of compact lattice QED

In the last section it was shown that a theory in order to be renormalizable has to show critical behavior at certain points in parameter space. The situation for QCD has already been mentioned above.

In the case of Abelian lattice gauge theory the situation is much more complicated. For a more detailed discussion see [20]. For large values of β, i.e. small values of the bare charge, these theories have properties which can

be proved by a perturbation expansion. In the case of QED this includes the massless photon field and the Coulomb force between static charges, up to higher order. So far this sounds satisfactory but as we decrease β below some critical parameter β_c, the theory exhibits properties quite different from those at large β. The expansion in this β-regime is called the strong coupling or high temperature expansion. In this phase, the *confining phase*, phenomena absent in the Coulomb phase, do occur: the gauge balls [21] acquire a non-zero mass, the static potential between static charges is directly proportional to the distance between them [12] and it amounts to the formation of monopole-antimonopole pairs [22].

Including charged fermion fields will bring about additional parameters to β. For the case of staggered fermions, leading to a 3-dimensional phase structure, see [23].

Here I will concentrate on Wilson fermions [24] with the additional parameter κ, which itself will depend on β at the critical point of the theory:

$$ma = \frac{1}{2}\Big(\frac{1}{\kappa} - \frac{1}{\kappa_c(\beta)}\Big). \tag{3.54}$$

Now the vacuum contains additionally a fermion condensate. Starting with

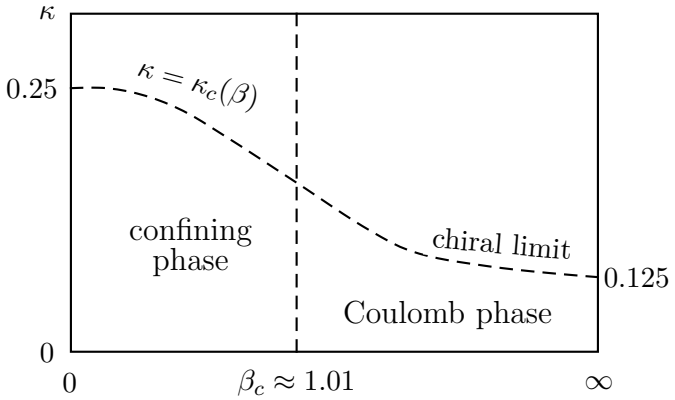

Figure 3.5: The phase structure diagram for compact lattice QED.

zero fermion mass leads to a spontaneous breaking of chiral symmetry, the fermions gain mass and furthermore a massless pseudoscalar Goldstone boson is present.

All these effects lead to two phases with totally different properties. For large values of β everything ever heard about Abelian gauge theories holds. But for small values of β the theory shows completely different properties similar to QCD. The two phases are separated by a phase transition in a

region where both, the weak and strong coupling expansion, break down. This happens at $\beta \simeq \beta_c$ where correlation lengths diverge. This is a point of non-analycity.

Many interesting questions emerge concerning the confinement phase and the phase transition. For example whether it is possible to construct a continuum theory preserving the properties from the confinement phase. If this is the case there would exist a continuum theory which has not yet been formulated as a lagrangian continuum theory. In order to push the continuum limit the theory needs a critical point. An obvious candidate would be the just mentioned phase transition. This point (and its immediate neighborhood) is accessible only by numerical methods. It is of great interest whether the phase transition is a continuous one or of first order. For the Wilson action it turns out that the transition is of weak first order [25–27] but still some calculations suggest a second order phase transition [20, 28]. For other actions the behavior at the phase transition is different.

Another thing of interest is the question whether the Landau pole problem could be solved. No Landau poles occur if the phase transition would be of second order. Other unexpected non perturbative results are obtained in the

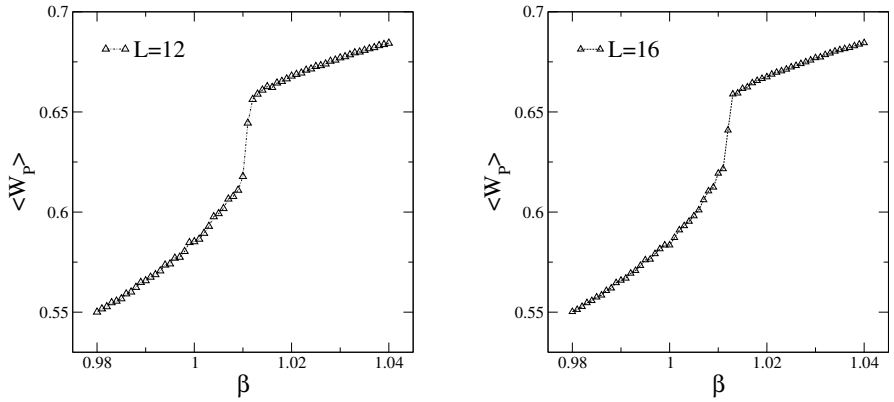

Figure 3.6: The plots show the behavior of the mean plaquette action $\langle W_P \rangle$ around the phase transition $\beta_c \simeq 1.011$ for two different lattices.

Abelian lattice gauge theory by including simultaneously scalar and fermion fields of the same charge, called the $\chi U \phi_4$-model [29].

From lots of calculations the critical point of the theory in the infinite volume limit was obtained to be $\beta_c \simeq 1.011$. This can also be seen in figure 3.6. Although the average plaquette action is not an order parameter, the steep increase is an indicator for critical behavior. Note, that the larger the

lattice becomes the more exactly the critical point is approached. This is of course what we expect because of finite size scaling.

In what follows the properties of zero modes and possible connections to gauge field topology are investigated. As we shall see, the zero modes only occur in the confining phase and thus it is of interest to know about the precise value of the critical coupling. For a calculation of β_c with high accuracy see [30].

3.7 Gauge field generation

The so-called Metropolis method is in principle applicable to any system and I will just talk about the basics. Suppose, we have a configuration C. Then we propose another configuration C' with a transition probability $P_0(C \to C')$ which only has to fulfill the following microreversibility requirement:

$$P_0(C \to C') = P_0(C' \to C). \tag{3.55}$$

In the case of a $U(1)$ gauge theory we suggest a new configuration by just choosing one of the link variables and multiplying it by $exp(i\rho)$, where ρ is random variable from $(-\pi, \pi]$. In this case (3.55) is clearly satisfied. The next step consists in the question whether C' should be accepted or not. The rule for making the decision is the following: if the action has been lowered, i.e. $exp(-S(C')) > exp(-S(C))$, then we accept the new configuration. In case the action has increased, the new configuration is accepted with probability P

$$P = \frac{e^{-S(C')}}{e^{-S(C)}}. \tag{3.56}$$

To this end a random number r from the interval $[0, 1]$ is generated. Then the new configuration is accepted if $r \leq P$. Otherwise we reject C' and keep the old configuration. It can be easily shown that this algorithm satisfies detailed balance and is ergodic [15]. It is used in general to update a single variable at a time.

The name overrelaxation stands for a particular way choosing the trial element for updating. The aim of the overrelaxation algorithm is to speed up the updating process. In this case a trial link variable is chosen far away from the original one such that the action remains invariant. A possibility then is to choose the new link as $U' = U_0 U^{-1} U_0$, with U_0 being an element of the chosen gauge group. This method changes individual links although the sum of plaquettes (and the action) remains unchanged. Hence the algorithm

is non-ergodic. Instead of the canonical ensemble, this algorithm creates the microcanonical ensemble with constant action. The main advantage of the overrelaxation algorithm is hat it can be used to counteract critical slowing down.

In practical computations these two algorithms are often used in common and alternating to take advantage of both.

Chapter 4

Dirac operators and the GWR

In the last chapter several solutions to overcome the fermion doubling problem and to obtain the correct continuum limit have been discussed. But they come with the unwanted concomitant effect of explicitely breaking chiral symmetry. An abandonment of other essential properties like unitarity and locality causes serious problems and hence usually chiral symmetry is sacrificed. However, in 1982 Ginsparg and Wilson wrote a paper [13] about the lattice equivalent of continuum chiral symmetry, embodied in the Ginsparg-Wilson relation, which will be the basis for the operators discussed in this chapter. Although it is not possible to fully retain chiral symmetry on the lattice some solutions which break chiral symmetry in a 'soft' local way appeared recently and are part of this chapter.

4.1 Ginsparg-Wilson fermions

Any chiral symmetric Dirac operator in the continuum limit satisfies the relation

$$\gamma_5 \mathcal{D} + \mathcal{D}\gamma_5 = 0. \tag{4.1}$$

As already mentioned, this relation is violated by all Dirac operators from the previous section because of the additional terms, which are necessary to remove the doublers. In order not to explicitly break chiral symmetry a new expression for the definition of chirality on the lattice is needed. In doing so, (4.1) is modified by a term which vanishes in the continuum limit as $a \to 0$ and we arrive at the Ginsparg-Wilson relation (GWR) in its original, full form [13]:

$$\gamma_5 \mathcal{D} + \mathcal{D}\gamma_5 = 2a\mathcal{D}\gamma_5 R \mathcal{D}. \tag{4.2}$$

Here a is the lattice spacing and R some local function of the gauge fields, which value depends on the chosen Dirac operator. It can be used to optimize

the spectral properties and often R is set to $1/2$, leading to an exactly circular spectrum. If the Dirac operator has no zero modes (4.2) can be rewritten in the following form

$$R = \frac{1}{2a}\gamma_5\{\mathcal{D}^{-1}, \gamma_5\} \tag{4.3}$$

and R can be seen as the measure of the amount of chiral symmetry breaking of the inverse Dirac operator. Obviously the term on the right hand side of (4.2), which causes the breaking of chiral symmetry, vanishes in the continuum limit. Thus, the chiral symmetry in the continuum limit is restored. The modification of the Ginsparg-Wilson relation corresponds to a modification of the chiral symmetry transformations (2.9) (see also [31])

$$\psi \to e^{i\epsilon\gamma_5(1-\frac{1}{2}aD)}\psi \qquad \bar{\psi} \to \bar{\psi}e^{i\epsilon(1-\frac{1}{2}aD)\gamma_5}. \tag{4.4}$$

Several operators are known to fulfill the Ginsparg-Wilson relation either exactly or approximately. Two of them, Neuberger's overlap operator and the so-called chirally improved operator, will be discussed in more detail here.

But afore some spectral properties of an operator satisfying (4.2) will be worked out.

- Suppose $|\psi\rangle$ to be an eigenvector of D with complex eigenvalue λ

  $$(\gamma_5 D + D\gamma_5)|\psi\rangle = (\lambda + \lambda^*)\,\gamma_5|\psi\rangle = (a\,D\,\gamma_5\,D)|\psi\rangle = a\,\lambda\lambda^*\gamma_5|\psi\rangle, \tag{4.5}$$

  where I have used the γ_5-hermiticity of D. Reforming the last equation yields

  $$\frac{2}{a}\mathrm{Re}\,\lambda = |\lambda|^2. \tag{4.6}$$

  As λ can be written as $\lambda = x + iy$ with x, y real, an equation describing a circle around $1/a$ is obtained

  $$\frac{2x}{a} = x^2 + y^2 \quad \Rightarrow \quad (x - \frac{1}{a})^2 + y^2 = \frac{1}{a^2}. \tag{4.7}$$

  Thus the Dirac operator has its eigenvalues on a circle around $\lambda = 1/a$. In the continuum limit, when a approaches zero, the circle becomes larger, meaning that the unphysical doubler region moves in this limit towards infinity and decouples from physical quantities.

- Consider an eigenvector ψ_e of the Dirac operator, satisfying the equation $D|\psi_e\rangle = \lambda|\psi_e\rangle$. Multiplying from the left with $\langle\psi_e|\gamma_5$ and using γ_5-hermiticity yields

  $$\langle\psi_e|\gamma_5 D|\psi_e\rangle = \lambda\langle\psi_e|\gamma_5|\psi_e\rangle = \langle\psi_e|D^\dagger\gamma_5|\psi_e\rangle = \lambda^*\langle\psi_e|\gamma_5|\psi_e\rangle. \tag{4.8}$$

  Thus $\langle\psi_e|\gamma_5|\psi_e\rangle = 0$ unless λ is real.

- Looking again at the equation $D|\psi_e\rangle = \lambda|\psi_e\rangle$ and making use of

$$D^\dagger = \gamma_5 D \gamma_5 \tag{4.9}$$

it is easily seen that

$$\langle\psi_e|\gamma_5 D = \langle\psi_e|\gamma_5\lambda^*. \tag{4.10}$$

But this means that the complex eigenvalues come in complex conjugate pairs λ, λ^*.

Applying the projection operator (2.12) to eigenvectors ψ_r corresponding to real eigenvalues, the zero modes, it is seen that

$$\langle\psi_r|\mathcal{P}_\pm|\psi_r\rangle = \pm 1 \tag{4.11}$$

and vanishes for non-zero eigenvalues.

Currently three formal solutions to (4.2) are known: Neuberger's overlap operator [32, 33], domain wall fermions [34] and the perfect actions [35, 36]. The only operator which can be constructed exactly is the overlap operator. The other operators obey the Ginsparg-Wilson relation only in certain limits. The overlap operator and its properties will be discussed in more detail in section 4.2. Aside from the above named solutions an approximate solution of (4.2) is also known. This is the chirally improved operator, which is a good compromise between chiral properties and computation time and will be discussed at length in the next section.

4.2 Overlap Fermions

A Dirac operator satisfying the Ginsparg-Wilson relation (4.2) preserves chiral symmetry on the lattice without fermion doubling. In general no ultralocal solution of the GWR does exist.

A few years ago Neuberger and Narayanan [32, 33, 37] came up with the idea of the *overlap* Dirac operator. Neuberger's overlap operator possesses the nice feature of realizing exact chiral symmetry on the lattice and it can be shown to have no fermion doubler modes. The massless overlap operator D_{ov} has the form

$$D_{ov} = \frac{1}{2}[1 + \gamma_5\epsilon(H_W)] \tag{4.12}$$

where H_W is some Hermitian Dirac operator, constructed from an arbitrary Dirac operator

$$H_W = \gamma_5(s - H_0), \tag{4.13}$$

and ϵ is the *sign* function. In general one uses for H_0 the usual Wilson Dirac operator with negative mass term and s is a real parameter in the range $|s| < 1$ which may be adjusted in order to minimize the probability for zero modes of $H_{\rm W}$. If H_0 is already an overlap operator $D_{\rm ov} = H_0$ for $s = 1$ because $\epsilon(\epsilon(H_{\rm W})) = \epsilon(H_{\rm W})$.

The sign function may be calculated [38] by the spectral representation

$$\epsilon(H_{\rm W}) = \sum_i \epsilon\lambda_i |\psi_i\rangle\langle\psi_i|, \tag{4.14}$$

where $|\psi_i\rangle$ denotes the $i^{\rm th}$ eigenvector. This definition cannot be used in practical computations because for realistic calculations the Dirac matrix is of size $\mathcal{O}(10^4 - 10^6)$. The overlap operator has to be used many times by entering diagonalization or conjugate gradient inversion tools and has to be constructed newly for each gauge field configuration. Thus, in practical implementations the *sign* function in (4.12) is calculated using

$$\epsilon(H) = \frac{H_{\rm W}}{|H_{\rm W}|} = \frac{H_{\rm W}}{\sqrt{H_{\rm W}^2}}. \tag{4.15}$$

One possible approximation of the inverse square root is to use Chebychev polynomials [39]. This method provides exponential convergence in $[\delta, 1]$, where δ (and thus the order of the polynomial) depends on the ratio of the smallest to largest eigenvalue of $H_{\rm W}^2$. For small δ a large number of terms is needed.

A non-locality in Neuberger's overlap operator can only arise from the inverse square root in (4.15). In the SU(3) case the authors in [40] calculated analytically bounds for the small field region and showed that Neuberger's operator is local with exponentially decaying tails. In the large field region the locality could not be guaranteed for all fields but the authors [40] were able to show that near zero modes of the inverse square root of (4.15) do not by itself imply non-locality.

4.3 Chirally Improved Operator

The numerical implementation of the fixed point Dirac operator and the overlap operator is a very (computation) time consuming and expensive task. Thus, a new attempt for solving the Ginsparg-Wilson equation has been suggested by [41, 42], called the chirally improved Dirac operator $D_{\rm CI}$. The idea is simply to expand the most general lattice Dirac operator in a series of simple basis operators on the lattice. As I have done some calculations on the $D_{\rm CI}$ its construction and some properties will be elucitated in more detail.

4.3.1 Expansion

The derivative term on the lattice is usually written as

$$\frac{1}{2}\sum_{\mu=1}^{4}\gamma_\mu\Big[U_\mu(x)\delta_{x+\hat{\mu},y}-U_\mu(x-\hat{\mu})^{-1}\delta_{x-\hat{\mu},y}\Big]. \tag{4.16}$$

But likewise we can write the derivative term having regard to all the symmetries as

$$\frac{1}{4}\sum_{\mu=1}^{4}\gamma_\mu\Big[U_\mu(x)U_\mu(x+\hat{\mu})\delta_{x+2\hat{\mu},y}-U_\mu(x-\hat{\mu})^{-1}U_\mu(x-2\hat{\mu})^{-1}\delta_{x-2\hat{\mu},y}\Big]. \tag{4.17}$$

As there are many more terms one could think of, an ansatz for the most general D must admit of a superposition of all discretization possibilities of the derivative term.

In (4.16) we find a single hop in positive μ-direction and a single hop in the negative direction, corresponding to the plus and minus signs. In (4.17) the hops are of length 2 and this can be continued to arbitrary lengths. In a short hand notation [42] a path of length n is denoted by

$$< l_1, l_2, l_3, \ldots, l_n >, \qquad l_i \in \{\pm1, \pm2, \pm3, \pm4\}. \tag{4.18}$$

With this notation and the $sign(l)$ abbreviated by $s(l)$ (4.16) and (4.17) can be written as

$$\frac{1}{2}\sum_{\mu}\gamma_\mu\sum_{l=\pm\mu}s(l)<l>, \tag{4.19}$$

and

$$\frac{1}{4}\sum_{\mu}\gamma_\mu\sum_{l=\pm\mu}s(l)<l,l>. \tag{4.20}$$

As we do not want the doublers to appear a term which distinguishes between the physical modes $p_\mu = 0$ and the doublers $p_\mu = \pi$ is needed. Such a term is included in the standard Wilson term and has to come with a $\mathbb{1}$ in spinor space. Further generalization of the Dirac operator means an inclusion of the remaining elements Γ_α of the Clifford algebra, i.e. tensors, pseudovectors, pseudoscalar. We end with the following form of the lattice Dirac operator [42]:

$$D=\sum_{\alpha=1}^{16}\Gamma_\alpha\sum_{p\in\mathcal{P}^\alpha}c_p^\alpha<l_1,l_2,l_3,\ldots,l_{|p|}>, \tag{4.21}$$

where the set $\mathcal{P}^\alpha$ consists of paths p with length $|p|$ and c_p^α being the complex weight correponding to p.

The next thing to do is to demand for some symmetries of D. We want to maintain translation and rotation invariance, invariance under charge and parity conjugation and additionally γ_5-hermiticity. The first thing, translational invariance is achieved through requiring the paths $\mathcal{P}^\alpha$ and their coefficients c_p^α to be independent of the starting point, whereas the rotation invariance requires a path and its rotated image have the same weight.Parity demands to include for each path p the parity-reflected copy with coefficient $s^\alpha_{\text{parity}} \cdot c_p^\alpha$. The signs s^α_{parity} are defined via $\gamma_4 \Gamma_\alpha \gamma_4 = s^\alpha_{\text{parity}} \cdot \Gamma_\alpha$.

More exciting is the inclusion of C and γ_5-hermiticity. Both of them relate the coefficient for a path p and its inverse p^{-1} together. Thus all coefficients c_p^α are restricted to be either real or purely imaginary. Furthermore, the coefficents for p and p^{-1} only differ in their signs, defined by $C\Gamma_\alpha C = s^\alpha_{\text{charge}} \cdot \Gamma_\alpha^T$, where T denotes transposition.

Collecting all the results we see that the paths in the ansatz group together and we obtain for the most general D (see also [43]):

$$
\begin{aligned}
D \equiv \mathbb{1}\Big[& s_1 + s_2 \sum_{l_1} < l_1 > + s_3 \sum_{l_2 \neq l_1} < l_1, l_2 > + s_4 \sum_{l_1} < l_1, l_1 > \dots \Big] \\
& + \sum_\mu \gamma_\mu \sum_{l_1 = \pm\mu} s(l_1) \Big[v_1 < l_1 > + v_2 \sum_{l_2 \neq \pm\mu} (< l_1, l_2 > + < l_2, l_1 >) \\
& + v_3 < l_1, l_1 > \dots \Big] \\
& + \sum_{\mu<\nu} \gamma_\mu \gamma_\nu \sum_{\substack{l_1=\pm\mu \\ l_2=\pm\nu}} s(l_1) s(l_2) \sum_{i,j=1}^{2} \epsilon_{ij} \Big[t_1 < l_i, l_j > \dots \Big] \\
& + \sum_{\mu<\nu<\rho} \gamma_\mu \gamma_\nu \gamma_\rho \sum_{\substack{l_1=\pm\mu, l_2=\pm\nu \\ l_3=\pm\rho}} s(l_1) s(l_2) s(l_3) \sum_{i,j,k=1}^{3} \epsilon_{ijk} \Big[a_1 < l_i, l_j, l_k > \dots \Big] \\
& + \gamma_5 \sum_{\substack{l_1=\pm1, l_2=\pm2 \\ l_3=\pm3, l_4=\pm4}} s(l_1) s(l_2) s(l_3) s(l_4) \sum_{i,j,k,n=1}^{4} \epsilon_{ijkn} \Big[p_1 < l_i, l_j, l_k, l_n > \dots \Big].
\end{aligned}
\tag{4.22}
$$

The γ_μ-matrices are chosen to be in the Euclidean chiral representation, i.e. $\gamma_\mu = \gamma_\mu^\dagger$, and hence all the coefficients s_i, v_i, t_i, a_i and p_i remain real. The ϵ's denote the totally anti-symmetric tensors with $2, 3$ and 4 indices, respectivly.

All paths in a group have the same length, are related by symmetries and must come with the same coefficient (up to sign factors).

In (4.22) only the leading terms of an infinite series of groups of paths is shown. Thus the dots in (4.22) indicate that longer paths are omitted. Actually an expansion of (4.2) contains infinitely many terms as it is known

that no ultra-local solutions of the Ginsparg-Wilson equation exists. Until the practical implementation starts, the chirally improved operator is kept in its most general form, i.e. no truncation is performed.

4.3.2 System of coupled equations and boundary conditions

Having expanded the lattice Dirac operator we can insert (4.22) into the Ginsparg-Wilson equation (4.2) and reform it to obtain

$$E \equiv -D - \gamma_5 D \gamma_5 + \gamma_5 D \gamma_5 D. \tag{4.23}$$

Now E is hermitean since D is γ_5-hermitean. An exact realization of the GWR would correspond to $E = 0$.

To find a solution to the linear part of E is no problem. A little bit more complicated is the computation of $\gamma_5 D \gamma_5 D$ but it can be done in a formally straight-forward manner. First the two elements of the Clifford algebra are multiplied together giving again an element of the algebra. Then the paths of the two terms have to be multiplied. This works quite comfortable in the above introduced short hand notation (4.18):

$$< l_1, l_2, l_3, \ldots, l_n > \times < l'_1, l'_2, l'_3, \ldots, l'_n > = < l_1, l_2, \ldots, l_n, l'_1, l'_2, \ldots, l'_n > . \tag{4.24}$$

In the case that two consecutive hops are opposed they cancel each other

$$< l_1, l_2, \ldots l_{j-1}, l_j, -l_j, l_{j+1}, \ldots, l_n > = < l_1, l_2, \ldots l_{j-1}, l_{j+1}, \ldots, l_n > . \tag{4.25}$$

Applying this rule all products of paths are reduced to their true length. Then the paths are rearranged with regard to their symmetry properties and one again ends up with an infinite series. From that series the coefficients, each itself representing an infinite series, are obtained. In order to find a solution of the Ginsparg-Wilson equation the left hand side of (4.23) must be zero. This means that the coefficients have to vanish simultaneously and we are left with the problem of solving a system of coupled equations. Before trying to solve the system of coupled equations we have to add boundary conditions on our system. This leads to two additional equations: one including only terms from the scalar sector and the other including only terms from the vector sector. An additional degree of freedom is added by introducing parameters $z_s(\beta)$ and $z_v(\beta)$. Each term in the boundary conditions is multiplied by a certain power of these parameters, making high order terms less important. The generalized boundary conditions take the form

$$0 = s_1 + 8 s_2 z_s + 48 s_3 z_s^2 + 8 s_4 z_s^3 \ldots \tag{4.26a}$$

$$1 = 2 v_1 z_v + 24 v_2 z_v^2 + 4 v_3 z_v^3 + \ldots \quad . \tag{4.26b}$$

The parameters are chosen such that they optimize the spectrum properties of D near the origin.

4.3.3 Truncation

The expansion of the most general D led to a system of coupled equations with infinitely many terms. The same is valid for the boundary conditions. Therefore an appropriate truncation of D is needed in order to leave a finite solvable problem. The arising question is where the truncation should be performed.

In the beginning of this section when expanding the most general D we have included paths of different length. Thus, the appropriate choice for a cutoff parameter is given by the length of paths in each term in (4.22). Figure 4.1 shows that the coefficients taken from table 4.1 roughly exhibit an exponential decrease. Hence the negligence of longer paths provides the searched cutoff parameter. Though a solution of the Ginsparg-Wilson cannot be ultra-local [44], locality is achieved if the Dirac operator $D_{x,y}$ decreases exponentially as $|x-y|$ increases. But there is also a practical part which

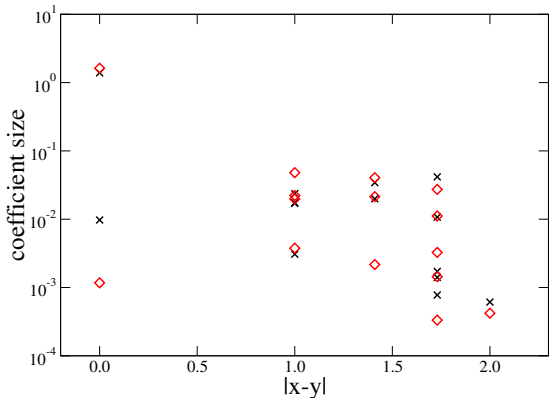

Figure 4.1: Half-logarithmic plot of the coefficients. The cross corresponds to the values obtained for $\beta \to \infty$, the diamonds to $\beta = 1.03$. The lattice size is 8^4.

justifies the truncation. Of course, the more terms one includes from (4.22) the better gets the approximation of the Ginsparg relation. But every new term included increases the computing time. So one has to make a satisfactory compromise between quality and numerical cost. It turned out that the storage cost lies below the ones of the overlap operator but above the ones of the usual Dirac operator.

At this place I add some remarks on the parameters and equations. A solution of all equations for a finite parametrization of the Dirac operator

would lead to an ultra-local solution. But this is not the case because the system of coupled equations is overdetermined and a solution can only be found for the leading terms, the path length again being the cutoff parameter.

After the truncation, leaving only paths with maximum length of 4 in lattice units, one is left with a set of 51 parameters (13 scalars, 18 vectors, 15 tensors, 4 pseudovectors, 1 pseudoscalar and z_s, z_v from the boundary conditions) and 99 equations (including the two boundary conditions). This is the starting position for further calculations.

4.3.4 Solving the system of coupled equations

Many lattice calculations involving the chirally improved Dirac operator have been done recently [38,41,42,45,46] for QCD and it turned out that the D_{CI} provides a completely alternative possibility to do lattice calculations within an acceptable amount of time and costs.

My aim was to implement D_{CI} for lattice QED. First of all I should mention that I was able to do some calculations in the Coulomb phase but didn't succeed in solving the system of coupled equations for the confining phase satisfactorily.

In order to obtain values for the huge set parameters for the chirally improved operator first of all I tried to find some similarity in the their behavior. To solve the system of coupled equations I have used the *Minpack*-package, providing several ways to deal with systems of non-linear, coupled equations, a conjugate gradient program and *Mathematica*. Especially *Mathematica* was quite handy to use when one already has a good idea for the starting values. In the free case, with all gauge links set to 1.0, a calculation and plot of the eigenvalue spectrum was quickly obtained. I started with a set of 6 parameters and continued by adding more and more parameters. For every new parameter I recommenced from the free case, slowly approaching the critical value of $\beta_c = 1.01$ until $\beta = 1.03$, where I still obtained good results for the parameters I have chosen. To match the number of expansion coefficients a new equation had to be included for every new parameter. The criterions for choosing these equations were:

- the equation which contains all parameters was always included;
  the boundary conditions (4.26a) and (4.26b) were always implemented

- in order to meet locality requirements of the Dirac operator the shortest paths should be more important then larger ones

- large coefficients of the parameters will give bigger contributions

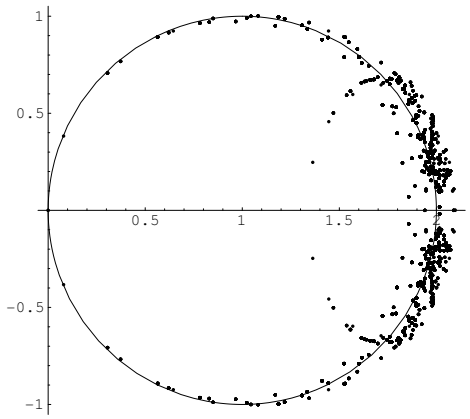

Figure 4.2: The free case, $\beta \to \infty$, all gauge links are set to 1, lattice size 8^4. The parameters are taken from table 4.1. Note, that near the origin, the region of physical interest, the eigenvalues lie on the Ginsparg-Wilson circle. The plot was done with *Mathematica*.

- linearly occurring parameters are more important, because all parameters (except the first one in the scalar sector) are (much) smaller than 1

Despite the above named criteria giving at least a short guide line, the equations have to be chosen very carefully because many combinations do not fit together.

The equations for the boundary conditions still contain some freedom for adjusting the spectrum. A reduction of z_s leads to a displacement of the spectrum on the real axis to the left and is used to adjust the spectrum so that it runs through the origin, corresponding to $m = 0$. A reduction of z_v stretches the spectrum in imaginary direction. Choosing these parameters identical led just in the case for big β ($\beta \approx 5$ and higher) to some proper results. The splitting between z_s and z_v becomes larger and larger as β reaches β_c. Actually one can impose boundary conditions also on the tensor, pseudovector and pseudoscalar sector [43], but this has only been done for the tensor sector without improving the result significantly.

Table 4.1 shows the parameter values for the free case and for two values of β near the phase transition. Figure 4.3 shows the physical interesting part of the spectrum close to the origin. All the above named results were actually easily obtained in the Coulomb phase.

The next step would of course lead into the confining phase. But this was not that easy. Going below $\beta = 1.03$ the spectrum started to shrink, the

	$\beta = \infty$	$\beta = 1.03$	$\beta = 1.05$
s1	1.390137	1.621192	1.620093
s2	-0.023669	-0.022216	-0.022109
s3	-0.019902	-0.021383	-0.021137
s5	-0.001719	-0.001435	-0.001421
s8	-0.003074	-0.003773	-0.003763
s10	-0.000612	-0.000420	-0.000410
s13	0.009736	0.001171	0.001663
v1	0.017454	0.019790	0.019665
v2	0.034295	0.040631	0.039696
v4	0.000776	0.003264	0.003362
v5	0.001406	-0.000333	0.000388
t1	0.000043	-0.002169	-0.001545
t2	-0.041665	-0.027316	-0.028861
t3	0.010719	0.011143	0.011073
t5	0.017047	-0.048020	-0.042481
z_s	1.0	0.963	0.973
z_v	1.0	0.883	0.878

Table 4.1: The first column shows the D_{CI} parameter values for the free case, whereas the other two columns show parameter values somewhat above the phase transition.

eigenvalues crowded in the middle of the Ginsparg-Wilson circle. Neither a big change in the adjusting parameters z_s and z_v nor choosing different parameters and sets of equations helped out of this dilemma. Also the above named criteria did not apply. It seems that the phase transition has big influence on the parameters. But as there are no general rules for selecting those one is quite lost.

What remains are some open questions and ideas which could eventually apply to the QED confining phase.

The phase transition seems to destroy the 'memory' of the parameters from the Coulomb phase. Maybe one has to start again with a small set of equations in the confining phase. Also other equations and parameters may become important and in general new criteria for selecting those should be chosen. Possibly two boundary conditions are too less and other ones may become relevant as well.

This was a short summary of the calculations and the results I did on the chirally improved operator. As already mentioned, without finding general

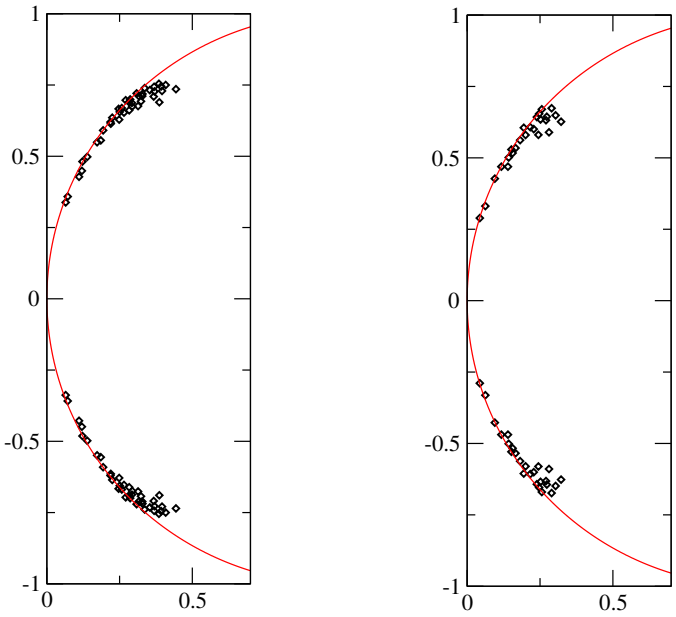

Figure 4.3: Results from 8^4 lattices. (a) shows the lowest 80 eigenvalues at $\beta = 1.05$. (b) shows the lowest 50 eigenvalues at $\beta = 1.03$. The circle indicates the GW-circle with radius 1 and center at 1.

applying rules for involving new parameters and/or equations, this is quite an extensive task. Nevertheless, spectrum information can be obtained in a much faster way than using the overlap operator and in a much more precise way than using only the usual Wilson operator.

Chapter 5

Technical part

In this chapter the motivation and technical background for the study of zero momentum modes is presented. First the topology of the gauge background is explored. Thereafter the essential features of zero-modes are discussed. Whenever possible a connection between those subjects will be established.

5.1 Motivation

The Atiyah-Singer index theorem [47] relates the topological charge of the background gauge field configuration to the number of fermionic zero-modes of the Dirac operator. A major progress in understanding the manifestation of the index theorem on the lattice was the realization that the eigenvectors of the lattice Dirac operator with real eigenvalues should be interpreted as the lattice counterparts of the continuum zero-modes (cf. collection of results in [48]). This can be understood from the fact that only eigenvectors ψ with real eigenvalues can have non-vanishing pseudoscalar matrix elements $\langle\psi|\gamma_5\psi\rangle$, like the zero-modes in the continuum.

The Atiyah-Singer index theorem states a particular connection between the background gauge field and the fermionic fields. Hence it is of interest to study the topology of the gauge background as well as the properties of the zero modes of the Dirac operator. The next step would be to look for possible connections between those.

In this chapter the background and technical details of both, the zero momentum modes and their possible relation to the gauge background are discussed.

5.2 Topology of the gauge background

In three dimensions a theory with internal symmetry group U(1) shows confinement for all values of β. This can be understood as the result of topological excitations [49,50]. Thus it is naturally to ask which topological artefacts are contained in 4-dimensional QED. In the next subsections topological objects of the gauge field configurations like monopoles, Dirac sheets and others will be discussed and possible connections to the zero mode occurence of the Dirac operator will be established. The authors in [51] conjecture that chiral symmetry breaking in compact lattice QED can be ascribed entirely to monopoles.

The appearence of confinement in three dimensions can be led back to the occurrence of magnetic monopoles. The search for monopoles makes use of Gauss's law. By measuring the total magnetic flux passing through a closed surface in the lattice we can determine whether or not the surface closes about a monopole.

As we shall see in the next section lots of effort have been invested in order to ascribe confinement in QCD to monopole condensation. In compact lattice QED, magnetic monopoles occur naturally in the confining phase. The study of those may serve to better understand the confining mechanism in QCD. The interested reader is refered to [51–56].

First we rewrite the Wilson action (3.11) in the form

$$S[U] = \beta \sum_{x,\mu>\nu} (1 - \cos\theta_{x,\mu\nu}), \tag{5.1}$$

where the link variable $U_{x,\mu} = exp(i\theta_{x,\mu}) \in U(1)$ and $\theta_{x,\mu} \in (-\pi, \pi]$. The plaquette angles are given by $\theta_{x,\mu\nu} = \theta_{x,\mu} + \theta_{x+\hat{\mu},\nu} - \theta_{x+\hat{\nu},\mu} - \theta_{x,\nu} \in (-4\pi, 4\pi)$.

Then the flux can be defined for small angles θ by [22]

$$ds \cdot B = \sum_{\text{surface}} ds_\mu \frac{1}{2} \epsilon_{\mu\nu\rho} (\nabla_\nu \theta_\rho - \nabla_\rho \theta_\nu) = \sum_{\text{surface}} \theta_{\text{P}}, \tag{5.2}$$

where θ_{P} is the oriented plaquette angle. According to this definition the net flux for any closed surface would be zero because each link appears twice, once with plus and once with minus sign.

Now we assume according to [22] that the plaquette angle $\theta_{x,\mu\nu}$ consists of a physical flux $\bar{\theta}_{x,\mu\nu}$ which lies in the range $(-\pi, \pi]$ and Dirac strings which carry 2π units of flux. Then we obtain

$$\theta_{x,\mu\nu} = \bar{\theta}_{x,\mu\nu} + 2\pi n_{x,\mu\nu}, \tag{5.3}$$

where $n_{x,\mu\nu} = 0, \pm 1, \pm 2$ is the number of Dirac strings passing through the plaquette $\theta_{x,\mu\nu}$. Plaquettes with $n_{x,\mu\nu} \neq 0$ shall be called *Dirac plaquettes*.

The monopole content of 3d cubes is obtained by simply counting the number of Dirac strings entering or exiting the cubes

$$2\pi M_{x,\rho} = \nabla_\sigma \epsilon_{\rho\sigma\mu\nu} \bar{\theta}_{x,\mu\nu} = 2\pi \epsilon_{\rho\sigma\mu\nu} \nabla_\sigma n_{x,\mu\nu}. \tag{5.4}$$

The middle part of (5.4) is the lattice equivalent of $M(x) = \vec{\nabla} \cdot \vec{B}$. Adding multiples of 2π to any of the link variables can move the Dirac strings but cannot change the net number entering or exiting a volume. From the above said it is clear that we have to choose the compact formulation of QED in order to extract the topology discussed here.

In close respect to the monopoles are the Dirac sheets. The dual integer valued plaquettes

$$n^*_{x,\mu\nu} = \frac{1}{2} \epsilon_{\mu\nu\rho\sigma} n_{x,\rho,\sigma} \tag{5.5}$$

form Dirac sheets bounded by the worldlines of monopole-antimonopole pairs. Dirac sheets can also be closed surfaces in the absence of monopoles and antimonopoles due to the periodic boundary conditions. Monopoles are topologically point-like objects in 3 dimensions and their worldlines on the dual lattice are closed, either within the lattice volume or by the periodic boundary conditions. A Dirac sheet in a 2-dimensional plane on a 4-dimensional lattice must contain at least $L \cdot L$ Dirac plaquettes.

In 4 dimensions the monopoles become 1-dimensional, and, due to the magnetic flux conservation, they form closed loops. Instead of (5.4) one can also calculate the net flux through the volumes

$$2\pi M_{\rho,x} = \frac{1}{2} \epsilon_{\rho\sigma\mu\nu} (\bar{\theta}_{\mu\nu,x+\sigma} - \bar{\theta}_{\mu\nu,x}), \tag{5.6}$$

where $M_\rho(x)$ can adopt the values $0, \pm 1, \pm 2$. It is clear that adding multiples of 2π to any of the link variables can move the Dirac strings but does not change the net number entering a volume. To count the monopoles in the whole system the monopoles from the subsystems (in my case cubes of unit volume) are simply added up.

The magnetic charge M, which is defined in (5.6) and has the following properties:

- M is quantized and assumes the values $0, \pm 1, \pm 2$
- In the case $M \neq 0$ there exist a magnetic current j.
- The monopole currents are conserved and form closed loops on the lattice. The loops are closed either by the lattice volume or by the periodic boundary conditions.

5.3 Zero modes of the Dirac operator

In chapter 4 we have seen that $\langle\psi|\gamma_5|\psi\rangle$ is zero unless the eigenvalue λ, satisfying $D|\psi\rangle = \lambda|\psi\rangle$, is real. Furthermore, applying the projection operator $\mathcal{P}_\pm$, defined in (2.12), we obtain the chirality ± 1 of the zero modes. Only exact zero modes should have definite chirality. For later convention a zero mode with $\langle\psi|\mathcal{P}_\pm|\psi\rangle = \pm 1$ is called right-(left-)handed.

Having obtained a lot of spectra we have to identify eigenmodes as zero modes. Using the overlap operator from the last chapter we know that the eigenvalues have to come in complex conjugate pairs (4.10) and are projected somehow on the unit circle. The real eigenvalues of the kernel Dirac operator in the physical part of the spectrum are projected to the left and characterized by having a zero imaginary part.

5.3.1 Localization properties of zero momentum modes

It is well-known in QCD that if we have an instanton configuration, the Dirac operator will show a zero mode localized in space-time around the center of the instanton [46, 57]. Nothing is known about the localization properties of zero modes in QED. In order to quantify the localization, gauge invariant observables, which inherit this localization, have to be consulted. To gain a bit more insight into the properties of these zero modes is subject of this chapter.

The simplest gauge invariant quantity which displays this localization is obtained by summing $|\psi(x,d)|^2$ over the Dirac indices d at each space-time point x. The lattice version of this scalar density $\rho(x)$ is given by

$$p(x) = \sum_d \psi(x,d)^* \psi(x,d) \equiv \psi^\dagger(x)\psi(x), \tag{5.7}$$

where $\psi(x,d)$ is an eigenvector of the lattice Dirac operator, normalized in a way that

$$\sum_x p(x) = 1. \tag{5.8}$$

For an eigenvector ψ, being a zero-mode of our Dirac operator, $\gamma_5\psi$ is also an eigenvector with $\gamma_5\psi = \pm\psi$ because as $\gamma_5^2 = 1$, the eigenvalues of γ_5 can only be ± 1. With this knowledge the so-called chirality is defined as

$$p_5(x) = \sum_d \psi(x,d)^* \gamma_5 \psi(x,d) \equiv \psi^\dagger(x)\gamma_5\psi(x), \tag{5.9}$$

The chirality actually provides a measure for the amount of chiral symmetry breaking because it takes on its largest value for the zero modes, namely

± 1, and is zero otherwise. Again it is assumed that the eigenvectors are normalized.

Of course one can define many more gauge invariant densities $p_\sigma(x)$ in the same manner as (5.7) and (5.9).

A convenient localization measure taken over from condensed matter physics, the so-called *inverse participation ration*, is introduced for further quantization of the localization (see for example [38]). It is defined as

$$I = V \sum_x p(x)^2, \tag{5.10}$$

where V is the volume of the lattice. To become acquainted with this variable a closer look at some extreme values I can take on may be helpful [58].

- I is largest if the whole contribution to the density results from one lattice point x. With the normalization condition (5.8) this states that

  $$p(x) = \delta_{xy} \quad \text{and} \quad p(x)^2 = \delta_{xy}. \tag{5.11}$$

  Summing $p(x)^2$ over all lattice points x we obtain 1 and thus the inverse participation ratio (5.10) is $I = V$.

- Now we assume the opposite case, namely the density is equally distributed on all lattice sites,

  $$p(x) = \frac{1}{V} \quad \text{and} \quad p(x)^2 = \frac{1}{V^2}. \tag{5.12}$$

  In this case the summation of $p(x)^2$ over all lattice points is V and the inverse participation ratio gives 1.

- Another case of interest occurs if we have n non-overlapping objects, each occupying a volume V_0 and $p(x) = r$ inside the volume. Outside of the volume $p(x) = 0$ and hence $r = 1/nV_0$. The inverse participation ratio now gives

  $$I = V \sum_{i=1}^{n} \frac{1}{n^2 V_0^2} = \frac{V}{nV_0^2} = \frac{1}{\rho V_0}, \tag{5.13}$$

  where $\rho = nV_0/V$ is the density of the objects. Note that for $\rho = const$, I should be independent of the volume V.

From the cases considered above we can conclude that the inverse participation ratio is large if the scalar density is localized and decreases to 1 the

more the density is spread out. Thus it is an appropriate measure for the localization of an eigenmode.

Analogously to (5.10) the pseudoscalar inverse participation ratio is defined by

$$I_5 = V \sum_x p_5(x)^2. \tag{5.14}$$

This is a measure for the localization of the pseudoscalar density $p_5(x)$. In the case of exact zero modes, I_5 is equal to I because $p(x) = |p_5(x)|$ for these configurations. This is because of the chirality of the zero modes which is ± 1. Generally it follows from (5.7) and (5.9) that

$$p(x) \geq |p_5(x)| \tag{5.15}$$

and from (5.10) and (5.14) we obtain

$$I \geq I_5. \tag{5.16}$$

If we consider an eigenmode corresponding to an eigenvalue far from the origin, $p_5(x)$ will be much smaller then $p(x)$ and fluctuate around zero. In this case I_5 is expected to be significantly smaller than I. But the closer the eigenvalues come to zero the more increases I_5 and the ratio I_5/I is expected to be close to 1.

5.3.2 Γ_σ densities

In the last section we have seen by looking at the inverse participation, a measure for localization, that we can expect clearly localized objects in the confinement phase of QED. As already mentioned there are more then only the scalar and pseudoscalar densities which one can consider. For every element of the Clifford algebra we can define a density in the same manner as (5.7) or (5.9)

$$p_\sigma(x) = \sum_d \psi(x,d)^* \Gamma_\sigma \psi(x,d) \equiv \psi^\dagger(x) \Gamma_\sigma \psi(x), \tag{5.17}$$

where Γ_σ denotes an element of the Clifford algebra (for the notation and numbering of Γ_σ see the appendix). The idea behind the calculation of the different densities is to see whether the right and left handed zero modes are sensitive to different topological sectors and whether there are interrelations between the different Γ_σ densities.

When analytically calculating $\langle \psi(x,d) | \Gamma_\sigma \psi(x,d) \rangle$ a certain correlation between the elements of the Clifford algebra Γ_σ is expected concerning the

$\langle\bar{\psi}\vert\Gamma_{15}\psi\rangle = +1$	$\langle\bar{\psi}\vert\Gamma_{15}\psi\rangle = -1$
$p_1 = p_{11}$	$p_1 = -p_{11}$
$p_2 = p_{12}$	$p_2 = -p_{12}$
$p_3 = p_{13}$	$p_3 = -p_{13}$
$p_4 = p_{14}$	$p_4 = -p_{14}$
$p_5 = -p_{10}$	$p_5 = p_{10}$
$p_6 = p_9$	$p_6 = -p_9$
$p_7 = -p_8$	$p_7 = -p_8$

Table 5.1: The table shows the interrelation between the densities of the different topological sectors, expected from the commutation relations between the Dirac matrices.

chirality of the eigenmodes. Table 5.1 shows the expected interrelation in the densities (5.17) between the Γ_σ's for different chirality. Note, that the usual used γ_5 is denoted by Γ_{15} now! The results in the table are simply obtained by using the anti-commutation relation for the Dirac matrices γ_μ and γ_5 (Γ_{15}).

Chapter 6

Results and Discussion

The first sections contain a summary of the results I have obtained by following the afore described methods and ideas. An attempt of interpretation and discussion of the results is attached. At the end of this chapter some visualization of the localization of modes is presented.

6.1 Gauge fields and Diagonalization

To obtain the background gauge fields I have used the Metropolis updating algorithm discussed in section 3.7. All configurations are well uncorrelated, separated by 5000 updating sweeps, each sweep consisting of 3 Metropolis and one overrelaxation step applied to every link on the lattice. Different values of β were used in the Coulomb phase as well as in the confining phase but most of the calculations were done for $\beta = 0.99$, just below the phase transition in the confining phase (this is actually only valid for a lattice size $\geq 8^4$).

For the values of β near the phase transition I have produced several hundred well uncorrelated configurations on the 4^4, 6^4 and 8^4 lattices and 100 on 12^4 lattices. The number of configurations deep in the confining phase and in the Coulomb phase was kept lower.

For the computation of the eigenvalues and eigenvectors the so-called implicitly restarted Arnoldi method [59] was used. This is a diagonalization routine for large, sparse non-hermitean matrices. As input operator I have used the overlap operator with the usual Wilson operator, built up from the before produced gauge field configurations, as kernel. From the overlap formalism (section 4.2) we know the physical part of the spectrum to be near the origin. Thus, only the lowest 12 eigenvalues and eigenvectors were calculated for the 8^4, 6^4 and 4^4 lattices, whereas on the 12^4 lattices the lowest 10 eigenvalues

were calculated. The search criterion for the eigenvalues was their modulus, meaning the computation of eigenvalues around the origin until the desired number and accuracy was achieved.

6.2 Zero mode statistics

In the next step it was of interest to look for exact zero modes of the Dirac operator. The criterion for identifying an eigenvalue as a real one was the condition, that the chirality is ± 1.

L	$\#_{\text{conf}}$	$n_0^{(0)}$	$n_0^{(1)}$	$n_0^{(2)}$	$n_0^{(3)}$	n_0^{tot}
4	400	397	3	0	0	3
6	400	376	24	0	0	24
8	500	323	173	4	0	181
12	100	36	44	15	5	89

Table 6.1: Number of zero momentum modes $n_0^{(\nu)}$ with degeneracy ν for different lattice sizes and $\beta = 0.99$.

L	$\#_{\text{conf}}$	$n_0^{(0)}$	$n_0^{(1)}$	$n_0^{(2)}$	n_0^{tot}
4	400	321	76	3	82
6	400	253	143	4	151
8	400	165	206	29	264

Table 6.2: Number of zero momentum modes $n_0^{(\nu)}$ with degeneracy ν for different lattice sizes and $\beta = 0.9$.

In the confined phase lots of zero modes were found whereas no zero modes appeared in the Coulomb phase. The zero-mode number is depicted in table 6.1 for $\beta = 0.99$ and in table 6.2 for $\beta = 0.9$. $n_0^{(\nu)}$ denotes the number of configurations showing n_0 zero modes with degeneracy ν. Thus, the total

number of zero modes of all configurations for a given lattice size is

$$n_0^{\text{tot}} = \sum_{\nu=1}^{\infty} \nu n_0^{\nu}. \tag{6.1}$$

For $\beta = 0.99$ the highest observed degeneracy was 3 on the 12^4 configurations. No zero modes were found in the Coulomb phase.

The small number of zero modes on the 4^4 lattices can possibly be ascribed to the fact that phase transitions on smaller lattices take place somewhat below β_c or that the lattice is to small and finite size effects become important.

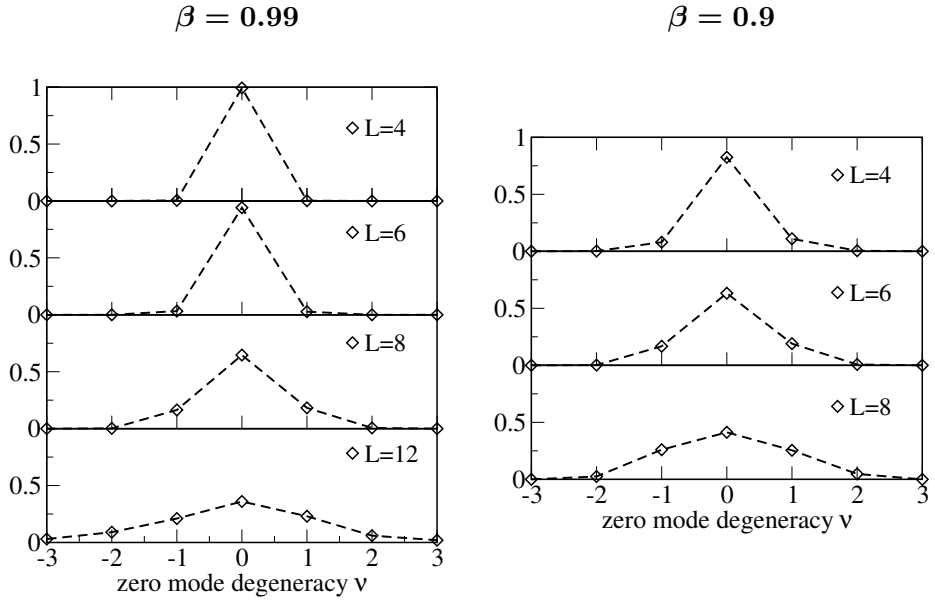

Figure 6.1: The plots show the number of zero momentum modes versus the zero mode degeneracy for two values of the inverse coupling. On the y-axis the number of zero modes is divided by the number of configurations.

The importance of finite size effects can be visualized even more clearly. Figure 6.1 shows the number of exact zero modes with plus or minus chirality for two different values of β. The scale on the x-axis denotes the degeneracy ν with the sign being the chirality ± 1. The scale on the y-axis represents the number of zero modes divided by the number of configurations. Clearly a volume dependence of the degeneracy of the zero modes is seen. The zero mode degeneracy is increased the more volume is available. This can be observed for both $\beta = 0.99$ and $\beta = 0.9$.

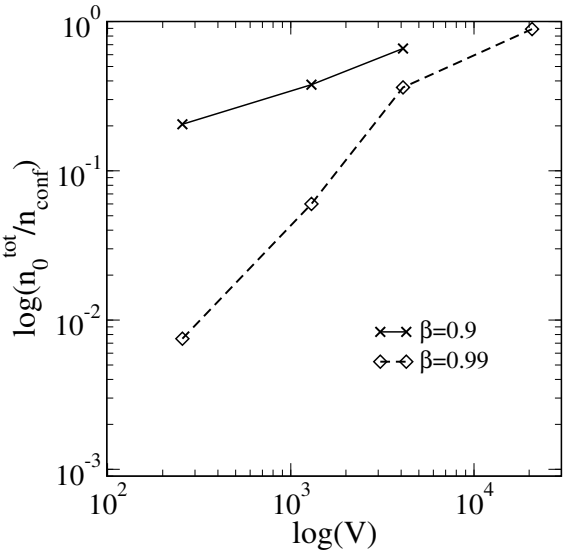

Figure 6.2: This figure shows the logarithm of the number of the zero modes normalized by the number of configurations versus the logarithm of the volume.

In figure 6.2 the total number of zero modes, defined in equation (6.1), divided by the total number of configurations is plotted against the volume in a double logarithmic plot for two values of β. Both lines tend to reach the value $n_0^{\text{tot}}/n_{\text{conf}} = 1$ as the volume increases. But this implies that in the infinite volume limit all configurations should exhibit zero modes. On the other hand this again supports the importance of finite size effects in small lattice volumes.

6.3 Monopole statistics

Having obtained the configurations exhibiting exact zero modes the next step was to look at the topology of the configurations themselves. Possible relationships between the zero mode degeneracy and the topological objects are tried to be established.

Following the definitions from section 5.2 the percentage of monopoles of the whole lattice volume was calculated. To obtain the correct normalization the monopole number is divided by $4 \cdot L^4$ because on the dual lattice the monopoles are one-dimensional objects and from equation (5.4) we see that we also have to take the four directions ρ into account. The number of Dirac plaquettes in a 2-dimensional plane is calculated as well. This quantity is called a Dirac sheet by the authors in [55]. As Dirac sheets defined in

L	ν	n_{Dp}/V	$\%n_m$
4	0	0.034(7)	6.15
4	1	0.075(52)	11.98
6	0	0.026(8)	11.90
6	1	0.028(9)	12.1
8	0	0.016(4)	11.88
8	1	0.016(5)	11.85
8	2	0.016(7)	11.2
12	0	0.0065(18)	11.75
12	1	0.0075(20)	11.90
12	2	0.0063(23)	11.85
12	3	0.0065(29)	12.13

Table 6.3: Percentage of monopoles $\%n_m$ of the whole lattice volume and number of Dirac plaquettes in a two-dimensional plane n_{Dp} per lattice volume for different lattice sizes and zero mode degeneracy ν at $\beta = 0.99$. The values in the table are averages over all configurations. The numbers in brackets denote the relative error.

equation (5.5) are gauge invariant objects I will refer to them simply as Dirac plaquettes. In the same step the magnetic charge M from equation (5.6) was calculated.

The results for the monopoles and Dirac plaquettes are shown in tables 6.3 and 6.4 for two different values of β in the confining phase. The second column denotes the zero mode degeneracy ν. At these β values a large number of monopoles was found. At $\beta = 0.99$ more than 10 percent of the lattice volume consisted of monopoles. This value is increasing as the coupling becomes stronger and at $\beta = 0.9$ we observe nearly 20 percent monopoles. All lattice sizes and topological sectors ν show nearly the same monopole percentage except the 4^4 lattice at $\beta = 0.99$. The reason was suggested in the last section and may be due to finite size effects or the smaller β_c value for smaller lattices.

The number of Dirac plaquettes slightly differs on the different lattices but is nearly constant for all topological sectors for a given lattice size.

L	ν	n_{Dp}/V	$\%n_m$
4	0	0.062(9)	19.40
4	1	0.064(18)	19.48
4	2	0.054(20)	18.93
6	0	0.027(8)	19.45
6	1	0.026(9)	19.38
6	2	0.034(13)	18.73
8	0	0.016(4)	19.56
8	1	0.016(5)	19.45
8	2	0.016(7)	19.28

Table 6.4: Percentage of monopoles $\%n_m$ of the whole lattice volume and number of Dirac plaquettes in a two-dimensional plane n_{Dp} per lattice volume for different lattice sizes and zero mode degeneracy ν at $\beta = 0.9$. The values in the table are averages over all configurations. The numbers in brackets denote the relative error.

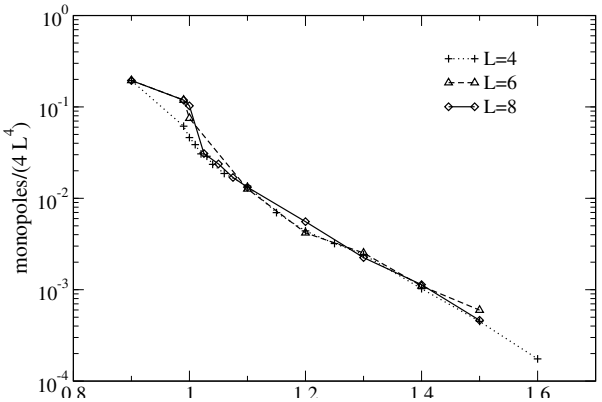

Figure 6.3: The plot shows the exponential suppression of monopoles in the Coulomb phase.

On the other hand the number of monopoles is exponentially decreasing (Figure 6.3) as β shifts through β_c but doesn't vanish completely until $\beta \approx 1.6$, depending on the lattice size. The stronger the coupling the more the

monopole number increases. As $\beta \to 0$ it is expected that the whole lattice volume consists of monopoles.

The same exponential decrease in the Coulomb phase was also observed for the number of Dirac plaquettes.

Concerning the magnetic charge it was found that for $\beta \approx \beta_c$ almost all monopoles have magnetic charge $M = \pm 1$. As a cross-check the net magnetic flux (see section 5.2) through the whole lattice volume was calculated and always obtained to be zero.

By looking at the tables 6.3 and 6.4 and comparing the values for different topological sectors obviously no clear correlations can be concluded. Some values are somewhat different from others but this may be due to the low statistics. We may draw the conclusion that no relevant relationship between the zero mode degeneracy of the Dirac operator and the occurrence of topological objects of the corresponding background gauge field at this stage can be established.

6.4 Density of the smallest eigenvalues

Interesting conclusions can also be drawn by the studies of the near zero modes and hence it may be worth to throw a short glance at those.

Chiral symmetry breaking is a key feature of the theory of strong interactions, QCD. This is accompanied by the creation of a chiral condensate $\langle \bar{\psi}\psi \rangle$. It is related to the density of eigenvalues $\rho(\lambda)$ of the Dirac operator at the origin via the Banks-Casher relation [60] and this in turn is related to the pion mass via the Gellmann-Oakes-Renner relation [61]. Compact lattice QED shows a confining phase for certain values of the coupling constant and hence we might also expect the appearance of a chiral condensate. The condensate is built up from the small eigenvalues and hence it was self-evident to look at the smallest eigenvalues of the Dirac operator.

The distribution of the smallest eigenvalue $p(\lambda_{\min})$ for a given lattice size L is obtained by binning the imaginary part of the eigenvalue and counting the number of eigenvalues in each bin. The result is shown in figure 6.4 for two different values of β and the topological sectors $\nu = 0, 1$. The exact zero modes have been left out. The sector $\nu = 2$ and the distribution for $L = 4, 6$ in the $\nu = 1$ have been left out because of the low statistics.

A common feature of all of the figures in 6.4 is that the smallest eigenvalues start to crowd near the origin as the lattice size increases and β decreases. In the sector $\nu = 0$ and $\beta = 0.9$, $p(\lambda_{\min})$ reaches zero already on 4^4 lattices whereas at $\beta = 0.99$ only larger lattices have eigenvalues near the origin. The distribution in the topological sector $\nu = 1$ is clearly farther from the origin

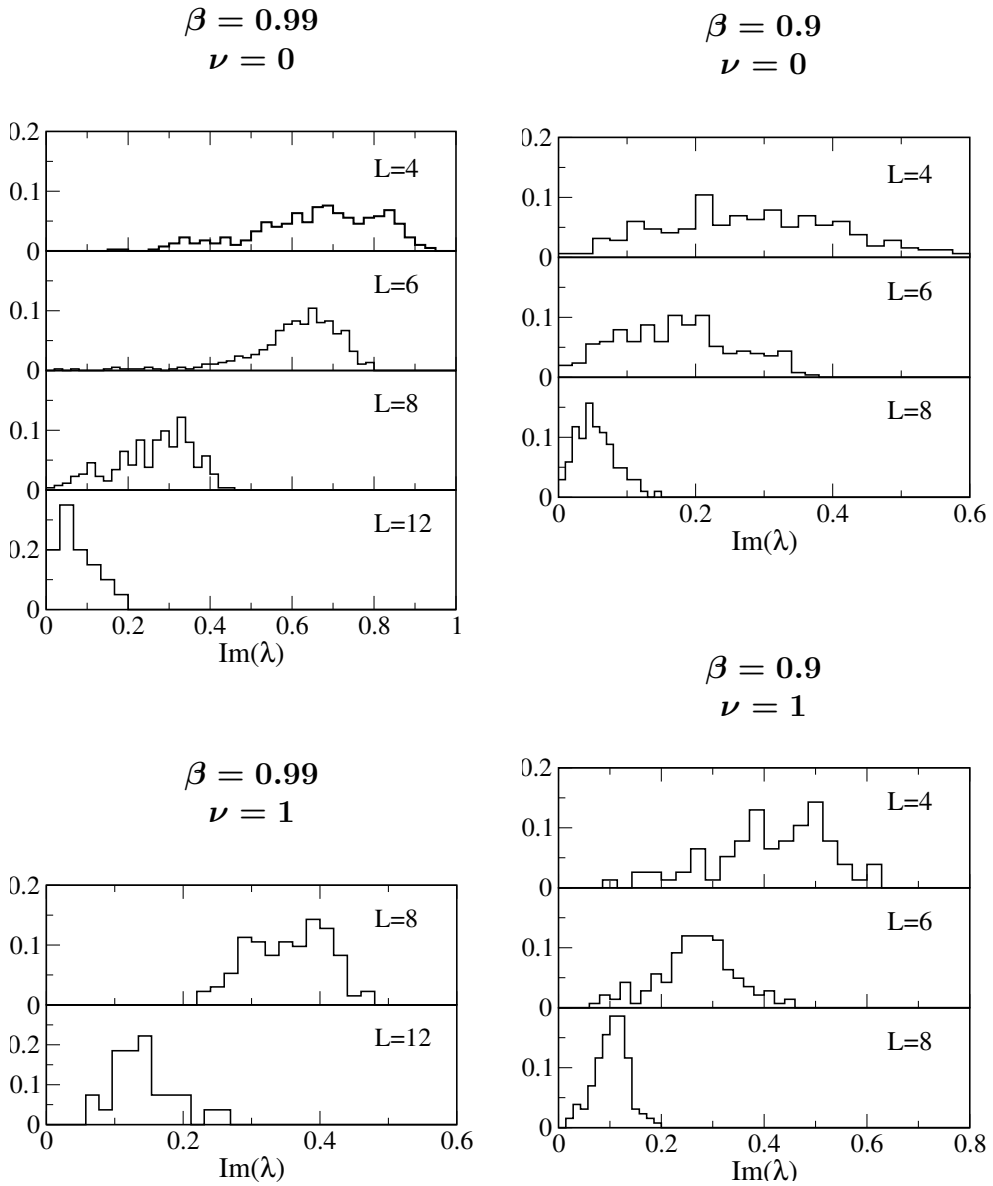

Figure 6.4: The plots show the distribution of the smallest non-zero eigenvalue $p(\lambda_{\min})$ on the y-axis versus the imaginary part of the eigenvalue. The left-hand plot (a) corresponds to $\beta = 0.99$ whereas the right-hand plot (b) represents the data at $\beta = 0.9$. Notice the difference in scaling on both axis.

then in the sector $\nu = 0$. This may be understood from the fact that the 'space' at the origin is already occupied by a zero mode (which have been left out in the distributions $p(\lambda_{\min})$) and is a typical feature in random matrix

theory.

From the presence of near zero modes very close to the origin the build-up of a chiral condensate is supported.

On the whole the distributions in figure 6.4 show a similar shape. This can be explained by random matrix theory, which predicts the statistical properties of the spectrum near the origin based on universality arguments [62]. For a study of the statistical properties of the low lying edge of the spectrum in lattice QED see for example [55, 56].

6.5 Localization

Until now it has not been checked whether the zero modes and near zero modes are localized or not. In subsection 5.3.1 the inverse participation ratio as a suitable measure for the localization of eigenmodes was introduced. In order to observe the predicted localization also the exact zero modes have been included.

The inverse participation ratio (5.10) is shown in figure 6.5. It is obtained by binning according to $\mathrm{Im}(\lambda)$. The obtained distributions are symmetric with respect to the real axis and hence only the part with $\mathrm{Im}(\lambda) > 0$ is shown. For all values of β and lattice sizes $\langle I \rangle$ is large in the vicinity of the origin, meaning that the zero and near zero modes are localized objects. It should be mentioned here that for single exact zero modes $\langle I \rangle$ reached values of about $5 - 7$, which is significantly larger than for the non-zero modes. Thus we can conclude in agreement with assumptions made in subsection 5.3.1 that the exact zero modes are localized are well localized objects.

The also mentioned pseudoscalar inverse participation ratio has not been calculated explicitely but its properties will be clear when discussing the results for the densities from different topological sectors in the next section.

6.6 Other densities

In subsection 5.3.2 it was pointed out that the scalar and pseudoscalar densities are not the only ones one can consider. Actually there are 14 more and the question is whether the left- and right-handed zero modes are sensitive to the different densities and if the expected interrelations from table 5.1 are fulfilled.

The definition of the Γ-matrices can be found in A.3. For the calculation of the densities equation (5.17) was used. Note, that Γ_{15} in this context is the

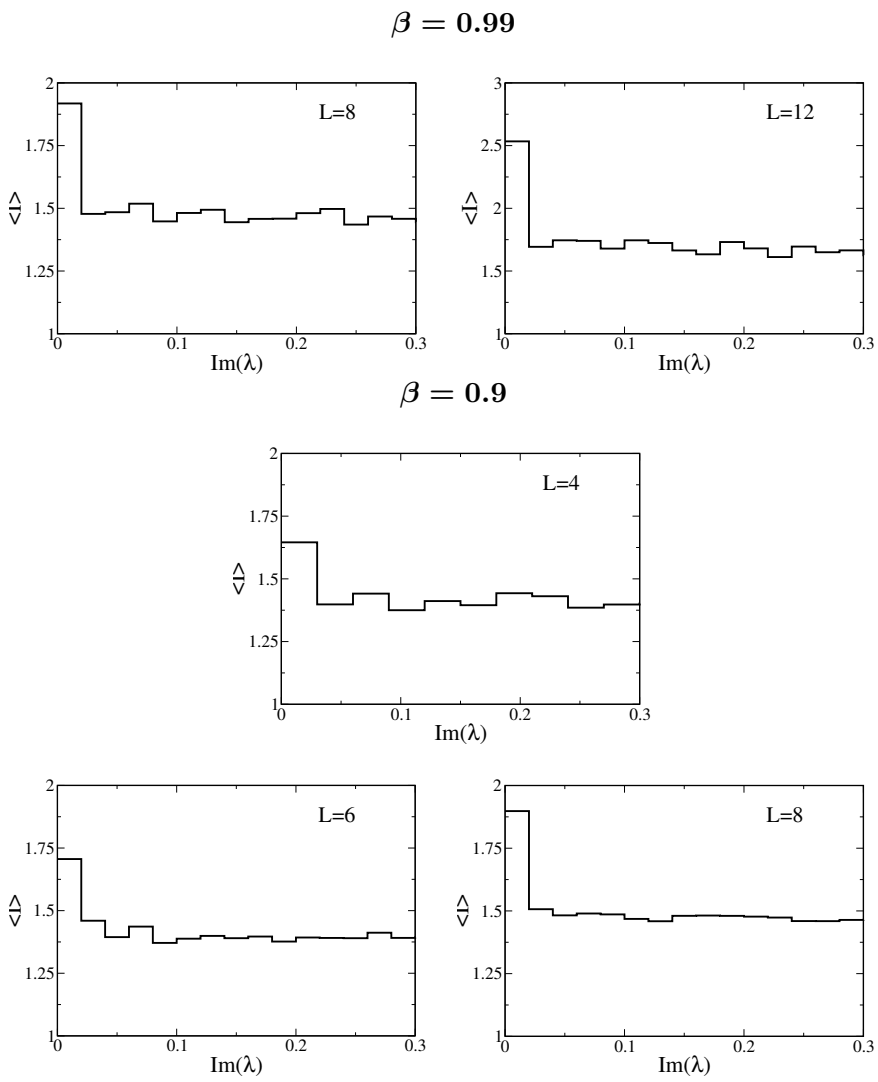

Figure 6.5: The graphs show the inverse participation ratio for different lattice size and different β. Notice the difference in scaling on the y-axis for the $L = 12$ lattice.

usual γ_5! In order to check whether the interrelations predicted in table 5.1 hold, certain densities are compared because they are expected to give the same result. If we consider for example an eigenmode with $\langle\psi|\Gamma_{15}\psi\rangle = +1$, it follows that $|\psi\rangle = |\Gamma_{15}\psi\rangle$ and thus e.g.

$$p_1 = \langle\psi|\Gamma_1\Gamma_{15}|\psi\rangle = \langle\psi|\Gamma_1|\psi\rangle. \tag{6.2}$$

The pseudoscalar density was obtained to be exactly ± 1 in case of exact

zero modes and zero otherwise. The densities in the vector $(p_1 - p_4)$ and in the axialvector $(p_{11} - p_{14})$ sector fulfill the relations predicted in table (5.1). They have zero magnitude in case of exact zero modes and take on values $\mathcal{O}(10^{-1} - 10^{-2})$ for non-zero eigenmodes.

The densities in the tensor sector $(p_5 - p_{10})$ adopt values $\mathcal{O}(10^{-1} - 10^{-2})$ in magnitude in case of zero momentum modes whereas the interrelations from table (5.1) are fulfilled.

For non-zero modes the predicted relations are not valid any longer in all sectors whereas the magnitude is $\mathcal{O}(10^{-1} - 10^{-2})$.

From the obtained results it can be concluded that the vector, tensor and axialvector sector are not very useful concerning the studies of localization properties. With the exception of the scalar and pseudoscalar density, there seems to be no clear sensitivity of the different Γ_σ's to the zero momentum modes.

To anticipate part of the next section, no clear structure in the 3-dimensional visualization of the respective density has been observed.

6.7 Visualization

In order to better understand the body structure of the occurring density objects it is desirable to have a visualization of these objects. The visualization of the 4-dimensional objects was performed by making 3-dimensional cuts through the lattice, namely in all 4 directions. Thus, on a L^4 lattice I obtained all in all $4 \cdot L$ $3d$ volumes, L in each direction. Then the $3d$ cuts in each direction have been joined into a movie in order to visualize the 'time evolution' of the density objects in certain directions.

The 3-dimensional cuts through the lattice and their visualization have been done with *IDL*. The picture sequence in figure (6.6) shows the evolution of the scalar density for the 4 directions on a 8^4 lattice. The density corresponds to an eigenvector of an exact zero-mode with positive chirality. For negative chirality states the density would not change in form, just in sign. The down-arrows point in the different directions of the evolution. Due to the periodicity of the boundary conditions the sequence does not end at picture 8 but starts at picture 1 again. The number on the right shows the order in which the pictures should be viewed and the arrows pointing to the right indicate the respective cut number for the different cuts. The density isosurface was chosen large enough to show the the dominating localized objects and small enough to not overwhelm the plot with background fluctuations. The value of the depicted isosurface is the same for all pictures showed in the sequence.

Evolution of the scalar density on a 8^4 lattice

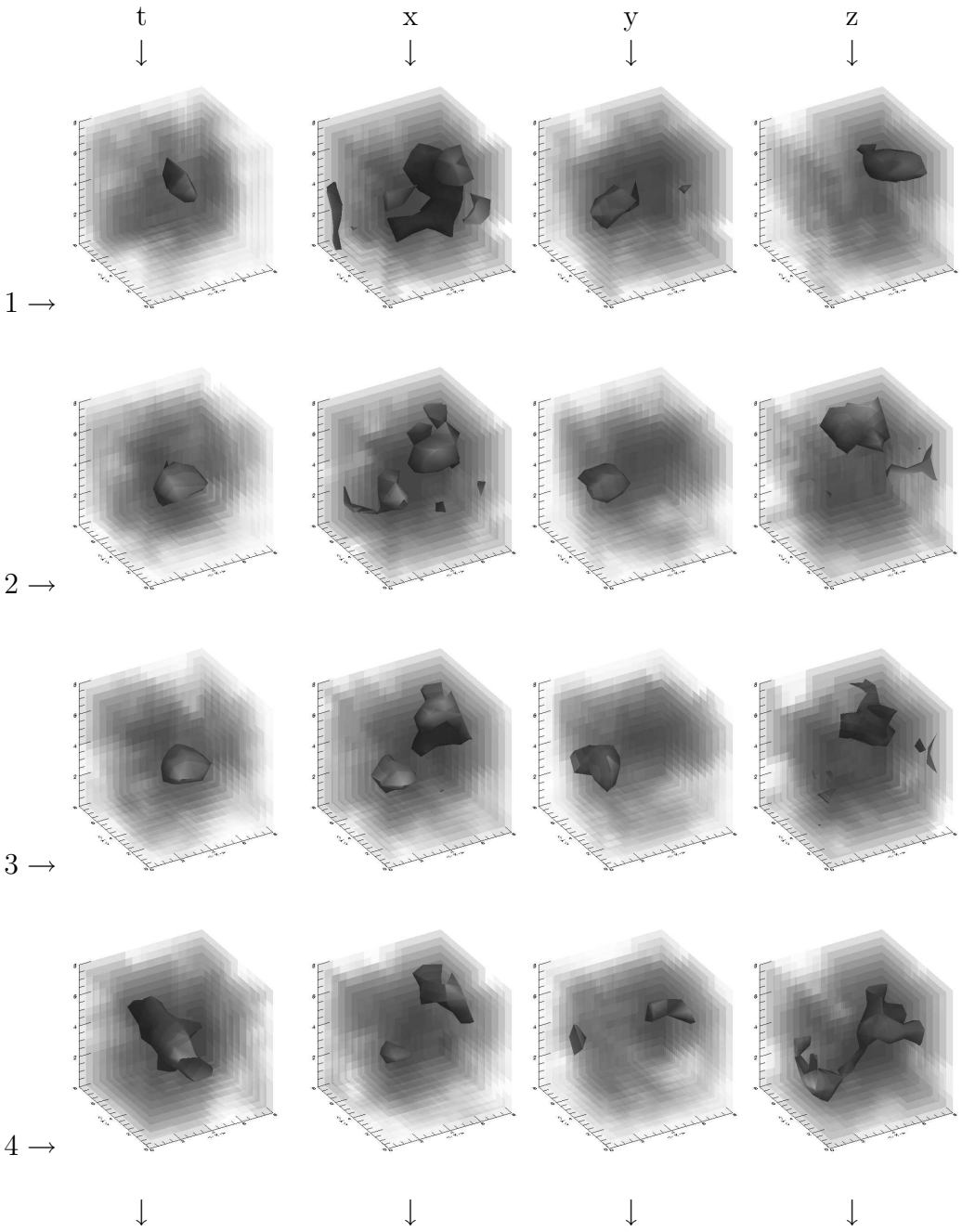

continue on the next page

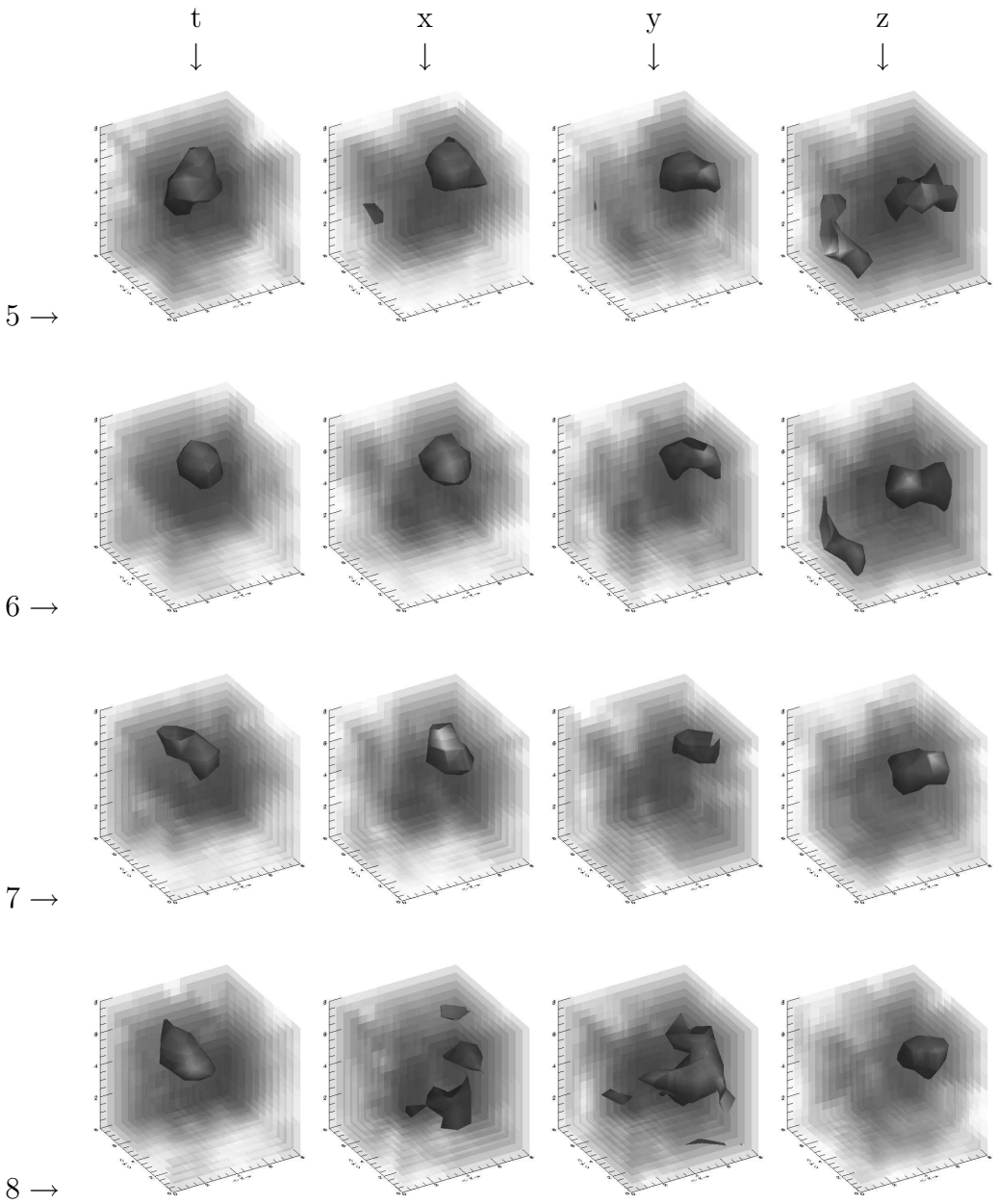

Figure 6.6: The four sequences show the 'time'-evolution for the scalar density for a zero-momentum mode with positive chirality. The down arrows denote the direction (x,y,z,t) in which the cuts 1...8 have been done.

Some structures occurring in the scalar density

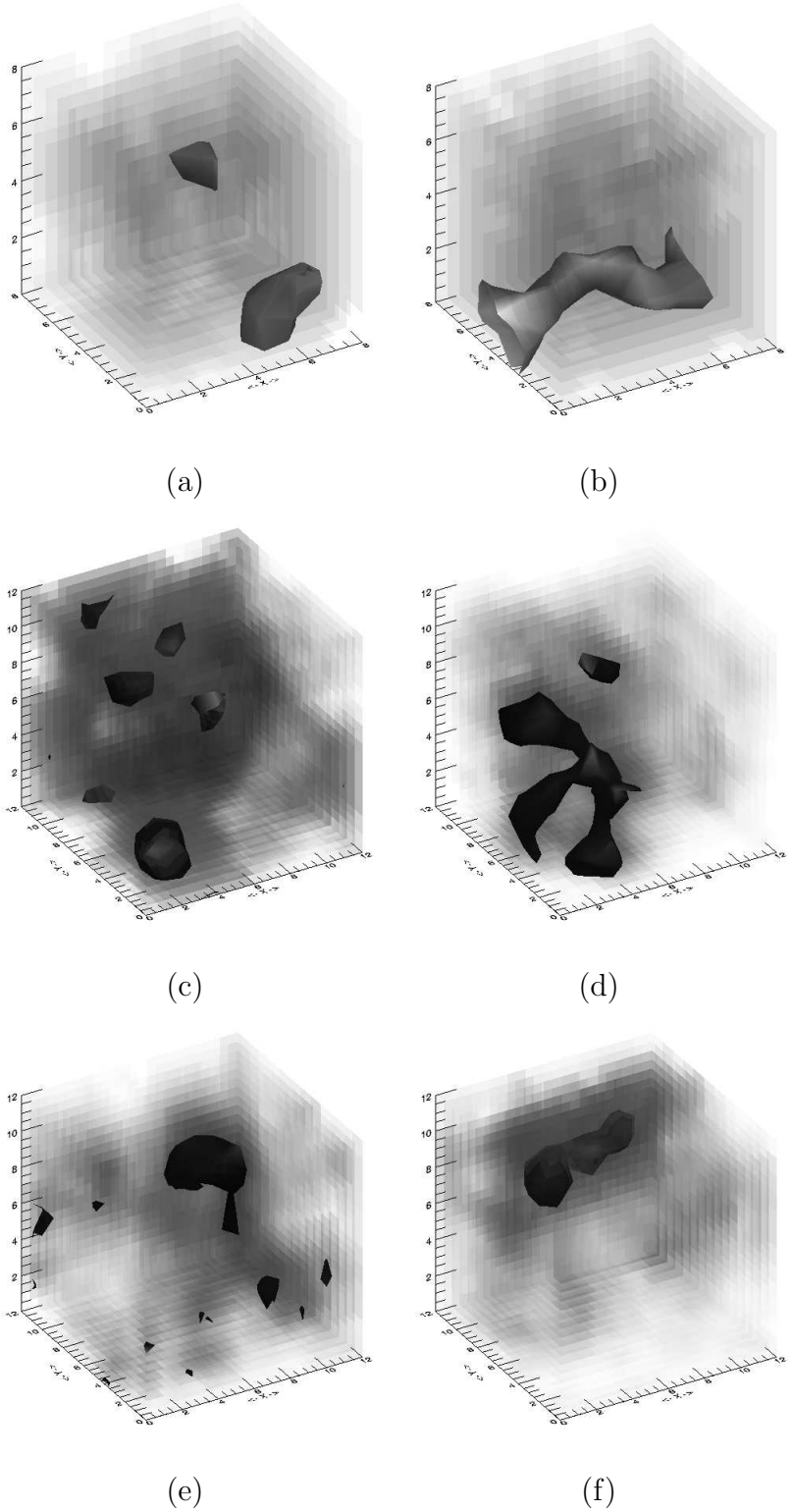

(a) (b)

(c) (d)

(e) (f)

Figure 6.7: The six plots show some density structures which frequently occur when cutting the scalar density. All graphs are obtained from exact zero modes. Figures (a) and (b) are from 8^4 lattices, whereas (c)-(f) are from 12^4 lattices.

Different topological objects are seen in these plots. There are clearly localized loop-like objects which are closed by the periodic boundary conditions. Localization in this context means that these object do not change very much in size and their position on the lattice. That these objects form closed loops on the periodic lattice can be seen if the sequences are used as a never-ending flip-book following the down pointing arrows. This might be the worldlines of monopole-antimonopole pairs. Follow for example the arrow pointing down in t- or y-direction. But there are also such objects which are not closed by the boundaries. Again making use of the flip-book, these objects will appear as a kind of pulsars.

In all observed sequences no direction was somehow outstanding concerning the structure, meaning that the anti-periodicity of the boundary conditions has no influence on the density.

For zero modes with definite chirality we have for the eigenvectors $\gamma_5|\psi\rangle = \pm|\psi\rangle$. Thus the density is equal for right-handed eigenmodes and differs in sign for the left-handed modes. This has also been observed.

Figure (6.7) shows some special objects which have been observed more or less often in the density structure. 6.7(a) shows two localized structures distinct from each other. Sometimes they are stable over some evolution steps and may connect to each other. The result is an 'elongated bubble' shown in 6.7(f). The larger the lattice the more separated localized objects occur. This can be seen on the cutout 6.7(c) from a 12^4 lattice. Quite often the localization is accompanied by a lot of fluctuations, which appear and vanish from one picture in the sequence to the next (see figure 6.7 and 6.7(e)). Objects, as depicted in 6.7(b) and 6.7(d), only occur very seldom, though they are very 'beautiful' in their structure.

Generally, the structures were observed to be much more distinct on the larger lattice volume. On 4^4 lattices the finite size effects made it almost impossible to detect a single localization. This confirms the results obtained from the inverse participation ratio, namely the increase of the localization as the lattice size increases.

Going to near zero modes and maybe even further away from the origin such structures do occur but only for a short part in the sequence. In this case it is almost impossible to speak about localization because these objects are hardly to distinguish from the increasing fluctuations.

The same procedure was repeated for configurations deep in the confining phase, at $\beta = 0.9$. Objects exhibiting the same structures do occur with an even narrower localization. On the other hand though their 'life-time' was much shorter than at $\beta = 0.99$.

Conclusive we may say that the localizations in the scalar density have been proved by eye, too, and the results obtained from the inverse participa-

tion ratio have been confirmed.

It should be mentioned here that the study of these visualizations has to be done by hand. Thus, only a short amount out of the huge set of eigenvectors has been elaborated and seen through. The results here may not have statistical significance, though the expected localization is confirmed and interesting graphical material to think about has originated.

6.8 Further checks on the topological objects

The confining phase of QED clearly shows well localized objects. In order to gain further insight into the occurrence and behavior of the different density objects, two tests concerning the behavior of the densities under a change in the gauge fields, were applied to the gauge fields.

First I have added a phase ϕ_μ to the link variables on each lattice site x, defined by

$$\phi_{x,\mu} = 2\,\pi\,n/L, \quad n = 1, \ldots, L, \quad \mu \text{ fixed} \tag{6.3}$$

where L denotes the lattice extension in the considered direction and μ can be one of the four euclidian space-time directions. Than, for a certain direction μ, the angle of the link variable is shifted to $\theta_{x,\mu} \to \theta_{x,\mu} + \phi_{x,\mu}$. The reason to do so was to eventually observe a kind of winding of the topological objects in 3 dimensions.

The link angle $\phi_{x,\mu}$ was added to $\theta_{x,\mu}$ in a single direction μ, whereas this was done for a fixed $\mu =$ (e.g. $\mu = 1$). This procedure was applied only to configurations exhibiting a zero mode. Such an additional phase leaves the plaquette action invariant. However, due to the finiteness there is no gauge transformation connecting the two systems. The characteristic polynomial coefficients of the eigenvalue equation involve traces over closed loops and thus may differ due to periodically closed loops. The number of monopoles and Dirac plaquettes did not change, either. Only the number of Dirac plaquettes was different for the gauge fields with the new phase.

The Dirac matrix was diagonalized again and the eigenvalues were compared with the ones without an added phase. The result was that the configurations with the new phase only sometimes showed the zero mode contained in the original configuration. This means that adding a phase in one direction will not always result in a configuration again exhibiting a zero mode.

When looking at the 3 dimensional density structure of the new eigenvectors we obtain a completely different picture, no matter in which direction the phase was added. Thus, changing $\theta_{x,\mu}$ in e.g. the t-direction will alter the density structure in the $x-, y-$ and $z-$direction as well.

Secondly, when discretizing the Dirac operator for a given gauge configuration the boundary conditions were changed from mixed-periodic to periodic ones. The idea was again to eventually observe a certain change in the density structure.

The eigenvalues and eigenvectors were calculated again and the corresponding densities were compared with the ones obtained from mixed-periodic boundary conditions. Also in this case the observed new 3-dimensional structure had no similarity with the old one at all. There was also a change in the monopole and Dirac plaquette number observable.

No certain pattern in the manner the density structure changes by adding a phase or changing the boundary conditions has been. Nevertheless, the structures do change and it will be part of future work to maybe find such a pattern.

Again this has to be done by hand and only a few configurations have been exploited.

Chapter 7

Conclusions and Outlook

The first practical part of my thesis consisted of searching for parameters for the chirally improved operator. This was possible for all values of β in the Coulomb phase, even quite close to β_c. Below the phase transition several problems prevented me to find suitable parameters keeping the eigenvalues on an approximate Ginsparg-Wilson circle.

The second step was to study the properties of the zero momentum modes and eventually exhibit a possible connection between the zero-mode degeneracy of the Dirac operator and the underlying gauge field configurations. To this end the eigenvalues and eigenvectors for the overlap operator were calculated. In the confined phase zero modes were found, its number depending on the lattice size and the value of the inverse coupling. Some statistics concerning the zero mode degeneracy of the Dirac operator at different values of β has been obtained.

For the pure gauge field part the monopole number and number of Dirac plaquettes were calculated for all gauge field configurations at different values of β, both, in the confining phase and in the Coulomb phase. A large number of monopoles and Dirac plaquettes was found in the confining phase.

Apart from the exponential decrease of monopoles and Dirac sheets and the absence of zero modes in the Coulomb phase no clear evidence for an interrelation between these topological objects and the number of zero modes of the Dirac operator was found. The obtained statistics suggests to the conclusion that magnetic monopoles play an important role in the confinement mechanism of lattice QED.

In a third step properties of the zero and near zero modes of the Dirac operator were computed. The smallest eigenvalues were binned according to their imaginary part. After having obtained this distribution the so-called inverse participation ratio was calculated. It provides a way to measure the localization of eigenmodes. The evidence for localization comes from an

increase of the inverse participation ratio for near zero modes. For exact zero modes it is significantly larger than for only near zero modes and hence the conclusion is that the exact zero modes are well localized.

The scalar density, included in the inverse participation ration, is only one out of 16 which have been calculated. The density $\langle\psi(x)|\Gamma_{15}\psi(x)\rangle$, representing the chirality of eigenmodes, was obtained to be exactly ± 1 for the right-(left-)handed zero modes. All other densities were obtained to fulfill certain interrelations but are not a skilled help concerning the study of localization properties.

After having found that the exact zero modes are well localized it is preferable to visualize these localizations. Therefore 3-dimensional cuts through the lattice were performed in order to get further insight into the localization properties of the eigenvectors. The above mentioned localization is certainly seen for values of β not too far beneath the phase transition and as long as the density $\langle\psi(x)|\Gamma_i\psi(x)\rangle$ is exactly ± 1, i.e. for exact zero modes. The stronger the coupling the smaller the localization of these objects. A lot of interesting structures did occur whereas they are not yet understood completely. Some of these objects were also closed by the periodicity of the boundary conditions and might be the worldlines of monopole anti-monopole pairs. Others showed clear localization but no closure within the lattice volume.

Two tests concerning a shift in the phase of the link variables have been applied to the gauge fields in order to further shed light on the structure of these objects.

Content of further studies may be to apply a cooling procedure to the gauge fields which could eventually remove the fluctuating background seen in the density pictures. This could in turn improve the localization.

The localization of the zero momentum modes has been shown by looking at the inverse participation ration and confirmed by their visualizations. Lots of structures did occur during the visualization whereby also a lot of new questions arose. Though the visualized densities have to be seen through by eye and hence their studies are quite time consuming, it may be helpful in order to get more insight into the localization properties of zero modes.

Appendix A

Technicalities

A.1 Elements of the Grassmann algebra

The mathematics or formalism to deal with anticommuting c-numbers was already developed by Grassmann in the latter half of the 19th century.

The Grassmann numbers are constructed from real or complex numbers and generators. For every fermion state we define a pair of *Grassmann variables* $(C_i, C_i^\dagger)$, which are called generators of an Grassmann algebra, if

$$\{C_i^\dagger, C_j\} = \{C_i, C_j\} = \{C_i^\dagger, C_j^\dagger\} = 0, \quad i, j = 1, \ldots N.$$

Note that $C_i^2 = 0$. In applications, we are interested in functions of products of η and $\bar{\eta}$, where

$$\eta = \psi C_i, \qquad \bar{\eta} = \bar{\psi} C_j.$$

ψ and $\bar{\psi}$ are Dirac c-number spinors and conjugate spinors. A general element of this algebra is defined as a power series in the η_i's. This power series has only a *finite* number of terms, i.e. for one η and one $\bar{\eta}$:

$$f(\bar{\eta}, \eta) = \sum_{n=0}^{\infty} f_n (\bar{\eta}\eta)^n = f_0 + f_1 \bar{\eta}\eta. \tag{A.1}$$

The coefficients f_n are assumed to be complex numbers. The addition of Grassmann numbers and multiplication with ordinary numbers is ensured by means of addition and scalar multiplication in any vector space. The main thing in dealing with Grassmann numbers is to integrate them. To define functional integration, we just need an analog of $\int_{-\infty}^{\infty}$. A given Grassmann variable η can at most appear to the first power in a function f. Therefore the following rules are sufficient to calculate an arbitrary integral:

$$\int d\eta_i = 0 \qquad \int d\eta_i \eta_i = 1.$$

In multiple integrals one has to keep in mind that the integration measures $\{d\eta_i\}$ anticommute among themselves as well as with all η_i's

$$\{d\eta_i, d\eta_j\} = \{d\eta_i, \eta_j\} = 0, \quad \forall i, j,$$

i.e. they are also Grassmann variables. $\eta^\dagger$ and $d\eta^\dagger$ are defined by the anti-commutator

$$\{\eta, \eta^\dagger\} = 0, \qquad \{d\eta, d\eta^\dagger\} = 0.$$

With these rules the integration of a function is defined as follows

$$\int d\eta\, d\eta^\dagger f(\eta^\dagger, \eta) = -\int d\eta^\dagger d\eta f(\eta^\dagger, \eta) \equiv f_1.$$

A simple application of this rule is

$$\int d\eta^\dagger d\eta e^{\lambda\eta^\dagger\eta} = \int d\eta^\dagger d\eta(1 + \lambda\eta^\dagger\eta) = -\lambda.$$

Another example shows the case with an additional pair of Grassmann variables $\bar{\xi}$ and ξ

$$\int d\bar{\eta} d\eta e^{-\lambda\bar{\eta}\eta + \bar{\xi}\eta + \bar{\eta}\xi} = \lambda e^{\lambda^{-1}\bar{\xi}\xi}.$$

Derivatives with respect to Grassmann variables can also be defined on the space of functions (A.1). Assume we want to differentiate $f(\eta)$ with respect to η_i. Then we define the following rules:

- $f(\eta)$ does not depend on $\eta_i \longrightarrow \frac{\partial}{\partial\eta_i} f(\eta) = 0$
- $f(\eta)$ depends on $\eta_i \longrightarrow$ define a left (right) derivative by bringing the variable η_i all the way to the left (right) and then apply the rule

$$\frac{\partial}{\partial\eta_i}\eta_i = 1 \quad \text{(left)}, \qquad \eta_i \frac{\overleftarrow{\partial}}{\partial\eta_i} = 1 \quad \text{(right)}. \tag{A.2}$$

Two examples should help to become confident with the above rules:

$$\frac{\partial}{\partial\eta_i}\eta_j\eta_i = -\eta_j \qquad i \neq j,$$

$$\bar{\eta}_i\, \eta_j \frac{\overleftarrow{\partial}}{\partial\bar{\eta}_i} = -\eta_j.$$

Notice that the integration over η_i is entirely equivalent to partial differentiation with respect to η_i,

$$\int d\eta_i f(\eta) = \frac{\partial}{\partial \eta_i} f(\eta).$$

Some applications, which are needed very often in field theory to deal with Feynman path integrals, are easily derived from what was said above about dealing with Grassmann variables and are discussed in Appendix A.2.

A.2 Functional Integrals

As an application of the integration rules for Grasmann variables we try to obtain a path integral representation of fermionic Green functions.
Consider the integral

$$Z[A] = \int \prod_{l=1}^{N} d\bar{\xi}_l d\xi_l e^{-\sum_{i,j=1}^{N} \bar{\xi}_i A_{ij} \xi_j}. \tag{A.3}$$

This can be rewritten as

$$e^{-\sum_{i,j=1}^{N} \bar{\xi}_i A_{ij} \xi_j} = \prod_{i=1}^{N} e^{-\bar{\xi}_i \sum_{j=1}^{N} A_{ij} \xi_j}$$

and since $\bar{\eta}_i^2 = 0$, only the first two terms in the expansion of the exponential will contribute, giving

$$e^{-\sum_{i,j=1}^{N} \bar{\xi}_i A_{ij} \xi_j} = (1 - \bar{\xi}_1 A_{1 i_1} \xi_{i_1}) \dots (1 - \bar{\xi}_N A_{N i_N} \xi_{i_N}).$$

The integration rules from Appendix A.1 imply that the integrand in (A.3) must contain the product of all Grassmann variables and therefore the only term to be considered is

$$G(\xi, \bar{\xi}) = \sum_{i_1, \dots, i_N} \xi_{i_1} \bar{\xi}_1 \xi_{i_2} \bar{\xi}_2 \dots \xi_{i_N} \bar{\xi}_N A_{1 i_1} A_{2 i_2} \dots A_{N i_N}.$$

The product of Grassmann variables in the above equation is antisymmetric under the exchange of any pair of indices and hence we may introduce the antisymmetric ϵ-tensor to find

$$G(\xi, \bar{\xi}) = \xi_1 \bar{\xi}_1 \xi_2 \bar{\xi}_2 \dots \xi_N \bar{\xi}_N \sum_{i_1, \dots, i_N} \epsilon_{i_1 i_2 \dots i_N} A_{1 i_1} A_{2 i_2} \dots A_{N i_N}.$$

But the expression under the sum is nothing other then the determinant and we get

$$G(\xi,\bar{\xi}) = (\det A)\xi_1\bar{\xi}_1\xi_2\bar{\xi}_2\ldots\xi_N\bar{\xi}_N.$$

Now we replace this expression in (A.3) to obtain

$$\int D(\xi\bar{\xi})e^{-\sum_{i,j=1}^{N}\bar{\xi}_i A_{ij}\xi_j} = \det A, \tag{A.4}$$

where the integration measure has the form

$$D(\xi\bar{\xi}) = \prod_{l=1}^{N} d\bar{\xi}_l d\xi_l.$$

Another integral which is needed quite often is the following one:

$$Z[\eta,\bar{\eta}] = \int \prod_{l=1}^{N} d\bar{\xi}_l d\xi_l e^{-\sum_{i,j=1}^{N}\bar{\xi}_i A_{ij}\xi_j + \sum_i(\bar{\xi}_i\eta_i + \bar{\eta}_i\xi_i)}, \tag{A.5}$$

where the sources $\{\bar{\eta}_i\}$ and $\{\eta_i\}$ now are elements of the Grassmann algebra as well. In order to evaluate (A.5) we first make a shift in the $\bar{\xi}_i$ and ξ_i variables

$$\bar{\xi}_i' = \bar{\xi}_i - \sum_k \bar{\eta}_k A^{-1}_{ki},$$

$$\xi_i' = \xi_i - \sum_k A^{-1}_{ik}\eta_k$$

and rewrite the integral (A.5) as follows

$$Z[\eta,\bar{\eta}] = \left(\int \prod_{l=1}^{N} d\bar{\xi}_l d\xi_l e^{-\sum_{i,j=1}^{N}\bar{\xi}_i' A_{ij}\xi_j'}\right) e^{-\sum_{i,j=1}^{N}\bar{\eta}_i A^{-1}_{ij}\eta_j}.$$

As the integration measure (A.2) is invariant under the above transformations and with the help of (A.4) we find that (A.5) finally becomes

$$Z[\eta,\bar{\eta}] = (\det A)e^{-\sum_{i,j=1}^{N}\bar{\eta}_i A^{-1}_{ij}\eta_j}. \tag{A.6}$$

What one now wants to do with these functional integrals is to differentiate them in order to obtain expectation values of fermion operators. To this purpose we look at integrals of the following type:

$$K_{i_1\ldots i_l i_1'\ldots i_l'}[A] = \int D(\bar{\xi}\xi)\xi_{i_1}\ldots\xi_{i_l}\bar{\xi}_{i_1'}\ldots\bar{\xi}_{i_l'}e^{-\sum_{i,j=1}^{N}\bar{\xi}_i A_{ij}\xi_j} \tag{A.7}$$

and show that

$$K_{i_1\ldots i_l i'_1\ldots i'_l}[A] = \prod_{l=1}^{N}\left\{\frac{\delta}{\delta\eta_{i_l}}\frac{\delta}{\delta\bar{\eta}_{i'_l}}\right\} Z[\eta,\bar{\eta}]\Bigg|_{\eta=\bar{\eta}=0}. \tag{A.8}$$

We start by expanding the exponential in (A.6) into a power series and making some careful resorting of the $\bar{\eta}$'s and η's by using the anticommutation rules for Grassmann variables. Then we apply the left and right derivatives (A.2) and finally obtain the important result

$$\begin{aligned}\int D(\bar{\xi}\xi)\xi_{i_1}\ldots\xi_{i_l}\bar{\xi}_{i'_1}\ldots\bar{\xi}_{i'_l}e^{-\sum_{i,j=1}^{N}\bar{\xi}_i A_{ij}\xi_j} \\ = (-1)^{l(l-1)/2}(\det A)\sum_P(-1)^{\sigma_P}A^{-1}_{i_1 i'_{P_1}}\ldots A^{-1}_{i_l i'_{P_l}},\end{aligned} \tag{A.9}$$

where the sum extends over all permutations

$$P: \quad \begin{pmatrix} i'_1 & i'_2 & \ldots & i'l \\ i'_{P_1} & i'_{P_2} & \ldots i'_{P_l} & \end{pmatrix}$$

and $(-1)^{\sigma_P}$ is the signum of this permutation.
As a particular case of (A.10) we obtain

$$\int D(\xi\bar{\xi})\xi_i\bar{\xi}_j e^{-\sum_{i,j}\bar{\xi}_i A_{ij}\xi_j} = (\det A)A^{-1}_{ij}. \tag{A.10}$$

from where we can define the two-point correlation function

$$\langle\xi_i\bar{\xi}_j\rangle = \frac{\int D(\xi\bar{\xi})\xi_i\bar{\xi}_j e^{-\sum_{i,j}\bar{\xi}_i A_{ij}\xi_j}}{\int D(\xi\bar{\xi})e^{-\sum_{i,j}\bar{\xi}_i A_{ij}\xi_j}}$$

and we obtain with help of (A.4) and (A.10)

$$\langle\xi_i\bar{\xi}_j\rangle = A^{-1}_{ij}.$$

This can be generalized to arbitrary correlation functions

$$\langle\xi_{i_1}\ldots\xi_{i_l}\bar{\xi}_{i'_1}\ldots\bar{\xi}_{i'_l}\rangle = \frac{\int D(\xi\bar{\xi})\xi_{i_1}\ldots\xi_{i_l}\bar{\xi}_{i'_1}\ldots\bar{\xi}_{i'_l}e^{-\sum_{i,j}\bar{\xi}_i A_{ij}\xi_j}}{\int D(\xi\bar{\xi})e^{-\sum_{i,j}\bar{\xi}_i A_{ij}\xi_j}}.$$

A.3 Euclidean definition of γ-matrices

Lattice field theory is done in Euclidean space-time. Hence the metric in Minkowski space-time $g_{\mu\nu}$ has to be replaced by a Euclidean one $\delta_{\mu\nu}$ It is convenient when doing lattice calculations in Euclidean space-time to also replace the usual Dirac matrices by a new set of γ-matrices $\gamma_\mu(\mu = 1, \ldots, 4)$, satisfying the algebra

$$\{\gamma_\mu, \gamma_\nu\} = 2\delta_{\mu\nu}. \tag{A.11}$$

The Euclidean γ-matrices are hermitean 4×4 matrices and I have used the following representation in my calculations:

$$\gamma_1 = \begin{pmatrix} 0 & 0 & 0 & -\mathbb{i} \\ 0 & 0 & -\mathbb{i} & 0 \\ 0 & \mathbb{i} & 0 & 0 \\ \mathbb{i} & 0 & 0 & 0 \end{pmatrix} \quad \gamma_2 = \begin{pmatrix} 0 & 0 & 0 & -1 \\ 0 & 0 & 1 & 0 \\ 0 & 1 & 0 & 0 \\ -1 & 0 & 0 & 0 \end{pmatrix}$$

$$\gamma_3 = \begin{pmatrix} 0 & 0 & -\mathbb{i} & 0 \\ 0 & 0 & 0 & \mathbb{i} \\ \mathbb{i} & 0 & 0 & 0 \\ 0 & -\mathbb{i} & 0 & 0 \end{pmatrix} \quad \gamma_4 = \begin{pmatrix} 0 & 0 & 1 & 0 \\ 0 & 0 & 0 & 1 \\ 1 & 0 & 0 & 0 \\ 0 & 1 & 0 & 0 \end{pmatrix}$$

The γ_5 matrix is defined in the following way:

$$\gamma_5 = \gamma_1\gamma_2\gamma_3\gamma_4 = \begin{pmatrix} 1 & 0 & 0 & 0 \\ 0 & 1 & 0 & 0 \\ 0 & 0 & -1 & 0 \\ 0 & 0 & 0 & -1 \end{pmatrix}.$$

γ_5 anti-commutes with all other Dirac matrices

$$\{\gamma_5, \gamma_\mu\} = 0 \tag{A.12}$$

and has the property

$$(\gamma_5)^2 = 1. \tag{A.13}$$

The commutators of the Dirac matrices define the $\sigma_{\mu\nu}$ matrices in the following way:

$$\sigma_{\mu\nu} = -\frac{i}{2}[\gamma_\mu, \gamma_\nu]. \tag{A.14}$$

$\sigma_{\mu\nu}$ is anti-symmetric in the indices μ and ν and therefore vanishes for $\mu = \nu$. Thus we obtain 6 σ matrices.

One more subset of matrices can be constructed by multiplying each γ_μ from the left by γ_5.

Thus, all in all, one is left with a set of 16 4×4 matrices, which are specified and named according to their symmetry properties:

scalar S:	$\Gamma_0 = \mathbb{1}$
vector V_μ:	$\Gamma_1 = \gamma_1$, $\Gamma_2 = \gamma_2$, $\Gamma_3 = \gamma_3$, $\Gamma_4 = \gamma_4$
tensor sector $T_{\mu\nu}$:	$\Gamma_5 = -\frac{\mathrm{i}}{2}[\gamma_1, \gamma_2]$ $\Gamma_6 = -\frac{\mathrm{i}}{2}[\gamma_1, \gamma_3]$, $\Gamma_7 = -\frac{\mathrm{i}}{2}[\gamma_1, \gamma_4]$,
	$\Gamma_8 = -\frac{\mathrm{i}}{2}[\gamma_2, \gamma_3]$, $\Gamma_9 = -\frac{\mathrm{i}}{2}[\gamma_2, \gamma_4]$, $\Gamma_{10} = -\frac{\mathrm{i}}{2}[\gamma_3, \gamma_4]$
axialvector A_μ:	$\Gamma_{11} = \gamma_5 \cdot \gamma_1$, $\Gamma_{12} = \gamma_5 \cdot \gamma_2$, $\Gamma_{13} = \gamma_5 \cdot \gamma_3$, $\Gamma_{14} = \gamma_5 \cdot \gamma_4$
pseudoscalar P_μ:	$\Gamma_{15} = \gamma_1 \cdot \gamma_2 \cdot \gamma_3 \cdot \gamma_4$

The capital Greek letters are the abbreviations I have used in the text and my programs. Note, that γ_5 is denoted by Γ_{15} now!

Appendix B

Acknowledgement

First of all I want to thank my family who made my whole education possible to me and were always a great support in all difficult situations.
Then I want to thank cordially my supervisor Univ.-Prof.Dr.Lang who always found some time to listen to all my suits and was a patient guide not only during the time writing my thesis but also through my whole studies.
Special thank is due to all members of the group for always having an open ear for refreshing discussions but still enough time for amusing jokes.
I also want to thank other members at the institute for always being helpful with all problems, both concerning physics or any other stuff.
I am very grateful to my colleagues and friends who did not choose the same path than me but always gave me the opportunity to expand my mind and knowledge to other fields.

List of Figures

List of Tables

Bibliography

[1] J.Horejsi, *Introduction to Electroweak Unification: Standard Model from Tree Unitarity*, World Scientific Publishing Company, 1994.

[2] A.Astbury, B.A.Campbell, F.C.Khanna, and J.L.Pinfold, *Topics in Electroweak Physics*, World Scientific Publishing Company, 1997.

[3] T-P.Cheng and L-F.Li, *Gauge Theory of Elementary Particle Physics*, Oxford University Press, 1988.

[4] F. Gross, *Relativistic Quantum Mechanics and Field Theory*, Wiley Science Paperback Series, 1993.

[5] E.G.Seiler, *Gauge theories as a problem of constructive quantum field theory and statistical mechanics*, Springer, 1982.

[6] R.P.Feynman, Rev.Mod.Phys. 20 (1948) 367.

[7] D.Bailin and A.Love, *Introduction to Gauge Field Theory*, Institute of Physics Pub, 1994.

[8] P.Ramond, *Field Theory: A Modern Primer*, Benjamin-Cummings Publishing Company, 1981.

[9] I. Montvay and G. Münster, *Quantum Fields on a Lattice*, Cambrige University Press, 1994.

[10] M.Göckeler et al., Phys.Rev.Lett. 80 (1998) 4119.

[11] M.Göckeler et al., Nucl.Phys.Proc.Suppl. 63 (1998) 694.

[12] K.G.Wilson, Phys.Rev. 10 (1974) 2445.

[13] P.H.Ginsparg and K.G.Wilson, Phys.Rev.D 25 (1982) 2649.

[14] H.B.Nielsen and M.Ninomiya, Nucl.Phys.B 185 (1981) 20.

[15] H.J.Rothe, *Lattice Gauge Theories: An Introduction*, volume 43, World Scientific Lecture Notes in Physics, 1992.

[16] R.Gupta, hep-lat/9807028 (1998).

[17] K.Jansen and C.Liu, Comput.Phys.Commun. 99 (1997) 221.

[18] B.Sheikholeslami and R.Wohlert, Nucl.Phys.B 259 (1985) 572.

[19] R.Gilmore, *Lie Groups, Lie Algebras and Some of Their Applications*, Krieger Publishing Company, 1994.

[20] J.Jersak, hep-lat/0010014 (2000).

[21] C.B.Lang et al., Nucl.Phys.B 499 (1997) 371.

[22] T.A.DeGrand and D.Toussaint, Phys.Rev.D 22 (1980).

[23] C.B.Lang et al., Nucl.Phys.B 532 (1998) 315.

[24] N.Zverev, *Algorithmic studies of compact lattice QED with Wilson fermions*, PhD thesis, Humboldt-Universität zu Berlin, 2001.

[25] I.Campos, A.Cruz, and A.Tarancón, Phys.Lett.B 424 (1998) 328.

[26] I.Campos, A.Cruz, and A.Tarancón, Nucl.Phys.Proc.Suppl. 73 (1999) 715.

[27] M.Baig, Nuc.Phys.Proc.Suppl. 42 (1995) 654.

[28] C.B.Lang, J.Jersak, and T.Neuhaus, Phys.Rev.Lett. 77 (1996) 1933.

[29] C.Frick and J.Jersak, Phys.Rev.D 52 (1995) 340.

[30] G.Arnold, T.Lippert, K.Schilling, and T.Neuhaus, Nucl.Phys.Proc. Suppl. 94 (2001) 654.

[31] M.Lüscher, Phys.Lett.B 428 (1998) 342.

[32] H.Neuberger, Phys.Lett.B 417 (1998) 141.

[33] H.Neuberger, Phys.Lett.B 427 (1998) 353.

[34] P.M.Vranas, Nucl.Phys.Proc.Suppl. 94 (2001) 177.

[35] P.Hasenfratz and F.Niedermayer, Nucl.Phys.B 414 (1994) 785.

[36] P.Hasenfratz, Nucl.Phys.Proc.Suppl. 63 (1998) 53.

[37] R.Narayanan and H.Neuberger, Nucl.Phys.B 443 (1995) 305.

[38] C.Gattringer et al., Nuc.Phys.Proc.Suppl. 206 (2002) 551.

[39] P.Hernández, K.Jansen, and L.Lellouch, Phys.Lett.B 469 (1999) 198.

[40] P.Hernández, K.Jansen, and M.Lüscher, Nuc.Phys.B 552 (1999) 363.

[41] C.Gattringer, Phys.Rev.D 63 (2001) 114501.

[42] C.Gattringer, I.Hip, and C.B.Lang, Nuc.Phys.B 597 (2000) 451.

[43] P.Hasenfratz et al., Int.J.Mod.Phys.C 12 (2001) 691.

[44] I.Horvath, Phys.Rev.Lett. 81 (1998) 4063.

[45] C. Gattringer et al., hep-lat/0307013 (2003).

[46] C.Gattringer and C.B.Lang, Comp.Phys.Comm. 147 (2002) 398.

[47] M.Atiyah and I.M.Singer, Ann.Math.93 139 (1971).

[48] C. Gattringer, I. Hip, and C. B. Lang, Nucl.Phys.B 508 (1997) 329.

[49] A.M.Polyakov, Nucl.Phys.B 120 (1977) 429.

[50] G. Hooft, Nucl.Phys.B 79 (1974) 276.

[51] T.Bielefeld, S.Hands, J.D.Stack, and R.J.Wensley, Phys.Lett.B 416 (1998) 150.

[52] W.Kerler, C.Rebbi, and A.Weber, Phys.Lett.B 348 (1995) 565.

[53] W.Kerler, C.Rebbi, and A.Weber, Phys.Rev.D 50 (1994).

[54] V.Grösch et al., Phys.Lett.B 162 (1985) 171.

[55] B.A.Berg, U.M.Heller, H.Markum, R.Pullirsch, and W.Sakuler, Phys.Lett.B 514 (2001) 97.

[56] B.A.Berg, U.M.Heller, H.Markum, R.Pullirsch, and W.Sakuler, Nucl.Phys.Proc.Suppl. 106 (2002) 592.

[57] C. Gattringer, M. Göckeler, C. B. Lang, P. E. L. Rakow, and A. Schäfer, Nucl.Phys.B 522 (2001) 194.

[58] S.Schäfer, *Chiral symmetry and hadronic measurements on the lattice*, PhD thesis, Universität Regensburg, 2002.

[59] R.B.Lehouqh, D.C.Sorensen, and C.Yang, *ARPACK User's guide*, SIAM, New Nork, 1998.

[60] T.Banks and A.Casher, Nuc.Phys.B 169 (1980) 103.

[61] M.Gell-Mann, R.J.Oakes, and B.Renner, Phys.Rev. 175 (1968) 2195.

[62] E.V.Shuryak and J.J.M.Verbaarschot, Nucl.Phys.A 560 (1993) 306.